Insights into the Antibacterial Mode of Action of Cress Polysaccharide-Mediated NiO Nanoparticles

Yusra Jamil
Abdul Wali Khan University Mardan
Mansoor Ali
Abdul Wali Khan University Mardan
Sajid Ali
drsajid@yu.ac.kr

Yeungnam University
Douglas Law
INTI International University
Abdulwahed Fahad Alrefaei
King Saud University
Ayaz Ahmad
Abdul Wali Khan University Mardan

Article

Keywords: Green-synthesis, Biocompatibility, Polysaccharides, NiO nanoparticles, Antibiotic resistance, Antibacterial mechanism, ROS, Human health

Posted Date: February 5th, 2026

DOI: https://doi.org/10.21203/rs.3.rs-8704769/v1

Additional Declarations: No competing interests reported.

Version of Record: A version of this preprint was published at Scientific Reports on March 24th, 2026.
See the published version at https://doi.org/10.1038/s41598-026-45381-9.

Abstract

The global rise in resistance of pathogenic bacteria to the available therapeutics poses a serious challenge to the healthcare system. Recent studies unveiled the antimicrobial potential of nanoparticles. Here, we demonstrate that biocompatible green-synthesized nickel oxide nanoparticles (NiO NPs) eradicate resistant pathogenic bacteria through a concerted mechanism involving ROS-induced oxidative stress, membrane damage, and DNA fragmentation. Green synthesis of cress (*Lepidium sativum*) seed mucilage polysaccharides-based NiO (CSP-NiO) NPs was validated through extensive characterization using UV-Vis, FTIR, XRD, SEM, and EDX. The CSP-NiO NPs exhibited excellent biocompatibility with minimal hemolytic activity (< 5% at 200 µg/mL) and a dose-dependent antibacterial activity against both Gram-positive (*S. aureus* and *C. tetani*) and Gram-negative (*E.* coli and K. *pneumoniae*) pathogenic bacteria, with zone of inhibition increasing from 2.5 ± 0.38 to 10.25 ± 0.58 mm and MIC values ranging from 25 to 50 µg/mL. Growth kinetic analyses demonstrated a dose-dependent suppression of bacterial proliferation, while DCFH-DA fluorescence revealed a 1.6 to 2.0-fold increase in intracellular reactive oxygen species (ROS) levels compared to the controls. The protein leakage assay indicated significant membrane disruption up to 46.23 µg/mL, and agarose gel electrophoresis demonstrated extensive DNA fragmentation at higher concentrations. Our findings establish CSP-NiO nanoparticles as potent, biocompatible antibacterial agents and a promising sustainable platform against antibacterial resistance.

1. Introduction

The increasing prevalence of antimicrobial resistance (AMR) has become a key global challenge in contemporary healthcare [1, 2]. According to recent estimates, approximately 70—75% of bacterial infections have become resistant to the most commonly prescribed antibiotics in medical procedures [3]. The global rise in antimicrobial-resistant pathogens has reoriented research interests towards finding effective and cost-effective alternatives [4]. In this context, nanoparticles have attracted significant attention due to their nanoscopic size and high surface-area-volume ratio, which promote extensive interactions with microbial and viral membranes [5, 6]. Multiple studies have shown that metals, such as silver (Ag), nickel (Ni), cobalt (Co), and their oxide-based nanoparticles, show a strong antimicrobial effect against a wide range of pathogenic bacteria [7, 8].

Nickel oxide nanoparticles (NiO NPs) have garnered attention over the past years due to their excellent physicochemical stability, magnetic behavior, and catalytic activity, along with the demonstrated therapeutic effects, such as wound healing, anti-inflammatory, and antibacterial [9]. Compared to other metal-oxide nanoparticles, NiO NPs have several advantages, including lower production cost, stability, environmental compatibility, and a wide optical bandgap of 3.6 4.0 eV [10]. These properties have widened their applications in biomedicine, particularly for site-specific drug delivery, bioimaging technology, and antimicrobials [11, 12]. Experimental findings indicate that the antibacterial effect of NiO NPs is primarily mediated by the release of Ni^{2+} ions, which absorb onto the bacterial cell surface through electrostatic interactions [13]. These interactions disrupt membrane structure, promote the

efflux of intercellular constituents, and disturb cellular homeostasis. Subsequently, elevated oxidative stress and genotoxic effects are introduced, ultimately triggering regulated bacterial cell death pathways [14, 15].

Numerous physical and chemical methods are used for nanoparticle fabrication; however, green synthesis is generally preferred due to its operational simplicity, economic viability, sustainability, and reduced environmental burden [16]. The green synthesis relies on naturally derived reducing and stabilizing agents, such as plant-based extracts, polysaccharides, proteins, amino acids, and vitamins, thereby eliminating the use of harmful synthetic chemicals [17, 18]. In view of this, polysaccharides have been identified as particularly suitable biogenic matrices for nanoparticle synthesis because of their intrinsic biocompatibility and biodegradability [19]. Structurally, polysaccharides consist of polymerized monosaccharide units and occur abundantly in nature [20]. The functional groups, such as hydroxyl, carboxyl, and aldehyde, are essential for the reduction of metal ions and stabilization of nanoparticles during the synthesis processes [21]. *Lepidium sativum* (cress) is a natural source of polysaccharides that has received interest due to its biochemical profile and wide therapeutic potential [22, 23]. When soaked in water, *L. sativum* seeds secrete a mucilaginous gel, consisting of approximately 90% non-starch polysaccharides and 10% starch. Previous studies have reported that polysaccharides isolated from cress seed mucilage exhibit a range of biological activities, including antibacterial, antihypertensive, antioxidant, hypoglycemic, and hypolipidemic [24–26].

In the current study, we applied an eco-friendly and sustainable approach for synthesizing biocompatible cress polysaccharide-based NiO NPs. The antimicrobial potential of the synthesized nanoparticles was evaluated against known Gram-positive and Gram-negative pathogenic bacteria. Furthermore, the underlying antibacterial mechanism was explored with particular emphasis on the role of oxidative stress at the nanoparticle-bacteria interface. Our results implicate reactive oxygen species (ROS) in antimicrobial mechanisms, and indicate that nickel oxide nanoparticles synthesized using cress seed polysaccharides (CSP-NiO NPs) could provide an effective and sustainable approach to combating microbial resistance.

2. Materials and Methods

2.1. Materials and Reagents

Cress seeds were obtained from a local market in Mardan, Pakistan, and confirmed by the Department of Botany at Abdul Wali Khan University Mardan, Pakistan. Nickel precursor, nitrate hexahydrate ($Ni(NO_3)_2.6H_2O$), Nutrient agar/broth, 2',7'- Dichlorohydrofluorescein diacetate (DCFH-DA), Triton X-100, bovine serum albumin (BSA), Bradford reagent, hydrogen peroxide (H_2O_2), ciprofloxacin, chloramphenicol, and other analytical grade reagents were purchased from recognized commercial suppliers. All the solutions were prepared using distilled water as a solvent.

2.2. Isolation and Purification of Polysaccharides

Cress seed mucilage was isolated following the procedure as outlined earlier [27, 28], with some adjustments. 20 g of seeds were immersed in 1 L of sterile water for 24 hours at room temperature with continuous agitation using a magnetic stirrer. The mucilage was collected through a muslin cloth filtration. The polysaccharides from the mucilage were precipitated using 75% ethanol and purified by centrifugation (5000 rpm, 20 minutes). The precipitated polysaccharides were then dried using a rotary evaporator, weighed, and stored at -20°C for further use.

2.3. Green synthesis of Nickel Oxide Nanoparticles (CSP-NiO NPs)

The green synthesis of NiO nanoparticles was achieved using cress seed mucilage polysaccharides as a natural reducing and stabilizing agent. Figure 1 depicts the eco-friendly synthesis process of NiO NPs employing the cress seed mucilage polysaccharide. 1 g of precipitated cress mucilage polysaccharides was dissolved in 50 mL of deionized water and heated to 60°C. Then, 50 mL of nickel nitrate hexahydrate (Ni $(NO_3)_2.6H_2O$) solution (0.1 mM) was added dropwise to the polysaccharide solution under continuous stirring for 2 hours. The formation of a grayish-black colloidal mixture indicated the CSP-NiO nanoparticles synthesis [29]. The mixture was centrifuged at 12000 rpm for 15 minutes to collect the precipitate. The pellet was subsequently resuspended in deionized distilled water and washed two to three times to eliminate residual impurities. Afterward, the pellet was subjected to drying and calcination at 300°C for 2 hours. The resultant nanoparticles were ground into a fine blackish-gray powder using a mortar and pestle and stored in an airtight vial for further characterization.

2.4. Characterization of CSP-NiO NPs

The physicochemical and morphological characteristics of the green-synthesized CSP-NiO nanoparticles were determined through the application of UV–Visible spectroscopy (UV-Vis), Fourier Transform Infrared Spectroscopy (FT-IR), X-ray Diffraction (XRD), Scanning Electron Microscopy (SEM), and Energy Dispersive X-ray Spectroscopy (EDX).

2.4.1 UV–Visible Spectroscopic (UV-Vis) Analysis

The bioreduction of Ni^{+2} ions and the successful formation of CSP-NiO nanoparticles were initially verified by an observable color change from light green to blackish-grey. The UV-visible absorption spectra of cress seed mucilage polysaccharide-mediated green synthesized CSP-NiO nanoparticles were recorded in the wavelength range of 200–800 nm using a UV-visible spectrophotometer (Shimadzu UV-1800, Japan), with distilled water used as the blank reference.

2.4.2 Fourier Transform Infrared (FT-IR) Spectroscopic Analysis

Fourier transform infrared (FTIR) spectroscopy was employed to identify the functional groups associated with CSP-NiO nanoparticles. The FTIR spectra were recorded using an FTIR

spectrophotometer (Nicolet 870) within the range of 400–4000 cm^{-1} using the KBr pellet method. The resulting absorption bands obtained were attributed to the corresponding functional groups and nickel-oxygen stretching vibrations.

2.4.3 X-ray Diffraction (XRD) Analysis

The XRD patterns were recorded using an X-ray diffractometer (Model D8, Germany) to determine the crystalline structure and phase purity of CSP-NiO nanoparticles. The diffraction pattern was obtained within a scanning range of 2θ = 10—80°, using copper Kα radiation (λ = 1.54 Å), conducted under controlled conditions. The resulting diffractogram was utilized to ascertain the crystalline phase and lattice planes. The mean crystalline size was evaluated from the characteristic diffraction peaks using the Scherrer equation mentioned below:

$$D = \frac{k\lambda}{\beta \cos\theta}$$

Where *D* represents the crystalline nanoparticle size, *K* is the Scherrer constant (0.9), *λ* denotes the wavelength of light employed for diffraction (λ = 1.54 Å), *β* signifies the full width at half-maximum (FWHM) of the diffraction peak, and *θ* refers to the Bragg angle [30].

2.4.4. Scanning Electron Microscopy (SEM) and Energy Dispersive X-ray Spectroscopy (EDX) Analyses

SEM was employed to interpret the size and shape of the green-synthesized CSP-NiO nanoparticles. The nanoparticle powder was mounted on conductive carbon tape (Nisshin model 731) and coated with a thin gold layer via sputter coating (Cressington, Model 108A). SEM imaging was performed using a Tuscan MIRA3 LMU microscope at 20 kV. The elemental composition of the nanoparticles was assessed through EDX analysis in the 0–10 keV range using the same microscope employed for SEM imaging.

2.5. Hemolysis Assay

The hemolytic assay was conducted to evaluate the biocompatibility of cress seed mucilage polysaccharides and CSP-NiO nanoparticles against human red blood cells (HRBCs). 5 mL of freshly collected blood from a healthy human donor, after getting written consent, was centrifuged at 1500 rpm for 15 minutes to get the red blood cell (RBC) pellet. The pellet was washed several times with autoclaved normal saline (pH 7.4) and resuspended in autoclaved phosphate-buffered saline (PBS) at a 1:3 proportion. Different concentrations of cress seed mucilage polysaccharide and CSP-NiO nanoparticles were added individually to 100 µL of the RBCs suspension and incubated at 37 ºC for 1 hour. After incubation, the samples were centrifuged at 3000 rpm for 10 minutes. The spectrophotometric analysis was performed at 570 nm after transferring 100 µL of the liquid phase into a micro-well plate. Positive and negative controls consisted of Triton X-100 (0.5%) and PBS. The percentage of hemolysis was calculated using the following formula:

$$Hemolysis\ (\%) = \frac{(Mean\ OD\ of\ Sample - Mean\ OD\ of\ PBS)}{(Mean\ OD\ of\ Positive\ control - Mean\ OD\ of\ PBS)} * 100$$

2.6. Bacterial Strains and Culture Conditions Used for Antibacterial Activity

The antibacterial potential of cress seed mucilage polysaccharide and CSP-NiO nanoparticles was tested against four antibiotic-resistant pathogens: the two Gram-positive bacteria (*Clostridium tetani* and *Staphylococcus aureus)*, and two Gram-negative bacteria (*Klebsiella pneumoniae* and *Escherichia coli*). These strains were obtained from the Pathology Department of Mardan Medical Complex, Pakistan, and cultured on nutrient agar. Before treatment, the bacterial strains were aseptically inoculated into 5 mL of nutrient broth and incubated for 24 hours at 37°C with continuous agitation to achieve a cell density of approximately 1×10^5 colony-forming unit (CFU/mL) equal to a 0.5 McFarland standard.

2.7. Agar Well Diffusion Assay

The antibacterial activity of cress seed mucilage polysaccharide and CSP-NiO nanoparticles was determined using the agar well diffusion method as described previously [31]. Briefly, 24-hour-old bacterial cultures were spread evenly over nutrient agar plates using sterile cotton swabs. Wells of 6 mm diameter were aseptically punched into the agar through an autoclaved well borer. Varying concentrations of cress seed mucilage polysaccharide and CSP-NiO nanoparticles (200, 100, and 50 µg/mL) were loaded into the wells and incubated under optimal growth conditions (37°C for 24 hours). Ciprofloxacin discs were used as a positive control, while wells containing only the solvent served as a negative control. After incubation, the antibacterial activity was evaluated by measuring the diameter of the inhibition zones (in millimeters) formed around the wells.

2.8. Determination of Minimum Inhibitory and Bactericidal Concentration (MIC and MBC)

The MIC and MBC of cress seed mucilage polysaccharide and CSP-NiO nanoparticles were determined following the previously reported method [32]. A 100 µL aliquot of cress seed mucilage polysaccharide and CSP-NiO nanoparticles in serially decreasing concentrations (200-1 µg/mL) was loaded into each well of a 96-well microplate having 100 µL of nutrient broth. Serial dilutions were prepared using a two-fold dilution method, and 100 µL of bacterial inoculum was loaded into the corresponding wells. Nutrient broth without bacterial culture served as a negative control, while chloramphenicol was used as a positive control. The microplate was incubated under optimal conditions (37°C for 24 hours), and optical turbidity at 600 nm was measured using a BioTek Microplate Spectrophotometer (USA) before and after incubation to validate the MIC values. The minimum inhibitory concentration endpoint was defined as the least concentration of each tested sample at which no noticeable bacterial growth was observed. To determine the MBC, 2 µL from the wells showing no visible growth was plated onto the nutrient agar plates and incubated at 37°C for 24 hours.

2.9. Bacterial Growth Kinetics

Bacterial proliferation was measured using a 96-well microplate. Each well was filled with nutrient broth containing 1 × 10^5 CFU/mL of bacterial culture and treated with either cress seed mucilage polysaccharide or CSP-NiO nanoparticles at concentrations of 50, 100, and 200 µg/mL. The microplate was incubated under optimal conditions at 37°C with continuous agitation at 130 rpm [33]. Following inoculation, the optical density at 600 nm was recorded at 5-hour intervals for up to 25 hours.

2.10. Quantification of Reactive Oxygen Species (ROS)

The reactive oxygen species (ROS) generated in bacterial cells were quantified using the 2',7'-Dichlorohydrofluorescein diacetate (DCFH-DA) method [34]. Bacterial cell suspensions standardized to 1 × 10^5 CFU/mL were incubated with varying concentrations (50, 100, and 200 µg/mL) of cress seed mucilage polysaccharide and CSP-NiO nanoparticles at 37°C for 6 hours under constant agitation. After incubation, the cultures were exposed to DCFH-DA (200 μM) and maintained in the dark for 1 hour. Cells treated with 1 mM hydrogen peroxide (H_2O_2) were the positive control for the ROS generation, while untreated cells were the negative control. The fluorescence intensity of dichlorohydrofluorescein (DCFH), indicative of intercellular ROS production, was measured at an excitation wavelength of 485 nm and an emission wavelength of 535nm. ROS levels were expressed as a percentage relative to the untreated control group.

$$\%ROS = \frac{Sample\ Fluorescence}{Control\ Fluorescence} \times\ 100$$

2.11. Protein Leakage Assay

Protein leakage from bacterial cells was assessed using the Bradford assay. Bacterial suspensions (1 × 10^5 CFU/mL) were treated with different concentrations (50, 100, and 200 µg/mL) of cress seed mucilage polysaccharides and kept at 37°C for 6 hours. After the incubation phase, the cultures were centrifuged at 3000 rpm for 10 minutes. Subsequently, 100 µL of each supernatant was mixed with 400 µL of the Bradford reagent and incubated in the dark at 37°C for 15 minutes. Cells treated with 0.1% Triton X-100 served as the positive control, whereas the untreated bacterial culture in broth was the negative control. The absorbance was recorded at 600 nm, and protein concentration was determined using a bovine serum albumin (BSA) standard curve [35].

2.12. DNA Damage Assay

A DNA fragmentation assay was carried out to determine the genotoxic effect of cress seed mucilage polysaccharide and CSP-NiO nanoparticles on bacterial cells [36]. The cultures were exposed to varying concentrations (50, 100, and 200 µg/mL) of the test samples for a period of 24 hours. Genomic DNA was isolated from each sample using the phenol-chloroform-isoamyl alcohol method. The purified DNA was combined with 5 µL of loading dye (bromophenol blue) and added onto a 2% agarose gel having 0.5 µg/mL ethidium bromide. Bacterial DNA samples were resolved by gel electrophoresis at a constant voltage of 70 V for 3 hours and visualized under UV light (Bio-Rad Gel Doc System).

2.13. Statistical Analysis

All the quantitative data were expressed as mean ± standard deviation, and procedures were repeated thrice for the sake of statistical analysis. Statistical analysis was implemented by employing One-Way ANOVA followed by a post hoc test by means of R software.

3. RESULTS

3.1. Green Synthesis of NiO Nanoparticles Using Cress Seeds Polysaccharides

Nickel oxide nanoparticles were successfully produced using polysaccharides extracted from *Lepidium sativum* (cress) seeds' mucilage, which acted as both capping and reducing agents during the nanofabrication. The reaction between polysaccharides and Ni $(NO_3)_2$ salt, carried out for two hours, resulted in a distinct color change from light green to blackish-grey, visually confirming the formation of cress seed polysaccharide CSP-NiO nanoparticles. This simple and environmentally friendly approach highlights the potential of natural biopolymers in the green synthesis of functional nanostructures.

3.2. UV-Visible Spectral Characterization of CSP-NiO Nanoparticles

The optical absorption of the CSP-NiO nanoparticles was studied by UV-Visible spectrophotometry in the spectral range 200–800 nm, as shown in Fig. 2. The absorption spectrum obtained was clearly defined with a peak at about 350 nm, which is characteristic of green-synthesized NiO nanoparticles.

3.3 FTIR Spectral Characterization of CSP-NiO Nanoparticles

Fourier-transform infrared (FTIR) spectra of CSP-NiO nanoparticles displayed different adsorption bands associated with the surface functional groups and the metal oxygen vibrations, as shown in Fig. 3. The broad absorption band near 3324 cm^{-1} is associated with the stretching vibrations of hydrogen-bonded -OH groups, which supports the presence of surface hydroxyls and residual polysaccharide-based components of the green synthesis. The absorption band detected near 1635 cm^{-1} was attributed to bending vibrations associated with surface-bound organic residues. The appearance of a distinct band in the lower wavelength region at around 570 cm^{-1} corresponds to metal-oxygen (Ni-O) stretching vibrations, thereby validating the production of CSP-NiO nanoaprticles. Collectively, the FTIR profile corroborates the formation of CSP-NiO and confirms the presence of surface-associated functional groups acquired during the polysaccharide-mediated stabilization.

3.4. Crystalline Structure of the CSP-NiO Nanoparticles

The crystalline structure of CSP-NiO nanoparticles was confirmed by X-ray diffraction analysis. The diffractogram (Fig. 4) displayed prominent peaks at 2θ values of approximately 37.4°, 44.1°, 51.3°, 60.9°, and 77.0°. These peaks correspond to the reported 111, 200, 202, 220, and 311 crystallographic planes, respectively, of the cubic NiO phase, confirming the successful fabrication of the NiO NPs. The primary crystallite size of the synthesized NPs was analyzed based on the main peaks of the diffraction by using the Scherrer equation (K = 0.9), which indicated domains of the nanometric size. It must be noted that the size of crystallites measured using XRD is an indication of the size of coherently diffracting domains and may not be similar to the larger aggregated structures observed under the microscope.

3.5. Surface Morphology and Elemental Composition of the CSP-NiO Nanoparticles

The surface morphology of CSP-NiO nanoparticles was observed by scanning electron microscopy (SEM) at various magnifications (Fig. 5a-g). SEM micrographs suggest that the synthesized material primarily consists of irregularly shaped, agglomerated clusters of particles with rough surface features. At lower magnification, the nanoparticles appear as small aggregates at the micron scale, but higher-resolution images reveal that these aggregates contain smaller nanoscale components. The agglomeration is often found in metal-oxide nanoparticles synthesized through green synthesis routes, which can be caused by high inter-particle interactions, hydroxylation of surfaces, and the deposition of polysaccharide-derived surface residues.

The elemental structure of the CSP-NiO nanoparticles was identified through energy-dispersive X-ray spectroscopy. The EDX spectrum indicated the presence of nickel (Ni) and oxygen (O) as the predominant inorganic elements, corroborating the NiO nanoparticles synthesis (Fig. 6). Moreover, the signals associated with carbon (C) were detected, likely resulting from the polysaccharide-derived surface residues or carbon tape employed during the SEM investigation. Minor trace elements, including Na, S, K, Cl, and Si, were also detected and are likely associated with residual precursor salts, or sample preparation, rather than indicating a distinct crystalline impurity phase.

3.6. Biocompatibility of the CSP-NiO Nanoparticles

The hemolytic effect of the cress seed mucilage polysaccharides and green-synthesized CSP-NiO nanoparticles was determined against freshly obtained normal human erythrocytes. The cytotoxicity was examined at different concentrations and expressed as ± percent hemolysis. No significant percent hemolysis was observed for cress seed mucilage polysaccharides and CSP-NiO nanoparticles at all the screening concentrations, as summarized in Fig. 7. The results showed that CSP exhibited 0.17 ± 0.32% hemolysis at 25 µg/mL, which increased to 1.90 ± 0.29% at 200 µg/mL, with a 50% cytotoxic concentration (CC_{50}) higher than 10,000 µg/mL. This suggests its compatibility as a stabilizing agent in nanoparticle synthesis. In contrast, the CSP-NiO nanoparticles showed the percent hemolysis, ranging from 1.12 ± 0.31% at 25 µg/mL to 5.02 ± 0.89% at 200 µg/mL, respectively. The CC_{50} value for CSP-NiO nanoparticles against human erythrocytes was recorded to be 2,861.22 µg/mL. These findings revealed

that the CSP-NiO nanoparticles are bio-friendly and safe for clinical use, as they showed no significant hemolysis at lower concentrations and only slightly hemolytic at higher concentrations.

3.7 Antibacterial Activity of CSP-NiO Against Resistance Pathogenic Strains

The antibacterial activity of cress seed mucilage polysaccharide (CSP) and CSP-NiO nanoparticles was evaluated against selected pathogenic Gram-positive and Gram-negative bacterial strains using the agar well diffusion method (Fig. 8). Both CSP and CSP-NiO nanoparticles displayed a dose-dependent antibacterial effect, with an increased zone of inhibition observed as the dose increased from 50—200 µg/mL.

For *S. aureus*, CSP produced inhibition zones of 1.25 ± 0.09 mm, 3.25 ± 0.88 mm, and 5.75 ± 1.93 mm at 50, 100, and 200 µg/mL, while CSP-NiO nanoparticles displayed enhanced activity with inhibition zones of 2.50 ± 0.66 mm, 5.50 ± 0.50 mm, and 9.00 ± 0.58 mm at the same concentrations. Similarly, against *C. tetani*, CSP-NiO nanoparticles displayed inhibition zones of 3.75 ± 0.52 mm, 5.25 ± 0.34 mm, and 10.25 ± 0.76 mm, which were consistently higher than those observed for CSP alone. In the case of Gram-negative bacteria, CSP displayed no detectable inhibition at 50 µg/mL towards *Escherichia. Coli* and *K. pneumoniae*, however, measurable inhibition was seen at higher concentrations. CSP-NiO nanoparticles demonstrated improved antibacterial effect against *E. coli*, exhibiting inhibition zones 2.50 ± 0.38 mm, 4.25 ± 0.53 mm, and 10.25 ± 0.58 mm, and against *K. pneumoniae* with zones of 3.75 ± 0.27 mm, 5.75 ± 0.77 mm, and 8.00 ± 0.50 mm at 50, 100, and 200 µg/mL, respectively. Ciprofloxacin, employed as a reference control, displayed substantially larger inhibition zones ranging from 21.9 ± 1.1 mm to 24.2 ± 1.0 mm, as expected for a standard antibiotic. Overall, the results demonstrated that CSP-NiO nanoparticles displayed a moderate dose-dependent antibacterial effect and consistently outperformed CSP alone, particularly against Gram-positive bacterial strains.

3.8 Minimum Inhibitory Concentration (MIC) and Minimum Bactericidal Concentration (MBC) of CSP-NiO Against Resistance Pathogenic Strains

The minimum inhibitory concentration (MIC) of cress seed mucilage polysaccharide (CSP) and CSP-NiO nanoparticles was evaluated to identify the lowest concentration required to inhibit bacterial growth completely. The antibacterial effect of CSP, CSP-NiO nanoparticles, and the reference antibiotic chloramphenicol in terms of MIC and MBC is displayed in Table 1.

CSP-NiO nanoparticles showed enhanced antibacterial activity in comparison to CSP alone. For Gram-positive bacteria (*S. aureus* and *C. tetani)*, the MIC of CSP-NiO nanoparticles was observed at 25 µg/mL, whereas the corresponding minimum bacterial concentration (MBC) was noted at 50 µg/mL. CSP alone showed relatively higher inhibitory and bactericidal concentrations, with minimum inhibitory concentrations (MIC) of 50 µg/mL and minimum bactericidal concentrations (MBC) of 100 µg /mL

against the same bacterial strains. Against the Gram-negative bacteria (*E. coli and Klebsiella pneumoniae*), CSP-NiO nanoparticles exhibited MIC values of 50µg /mL and bactericidal activity at 100 µg/mL. CSP required higher concentrations to achieve both an inhibitory and bactericidal effect, as demonstrated by MIC and MBC values of 100 µg/mL against the tested Gram-negative strains. Chloramphenicol, a reference control, displayed low minimum inhibitory concentration (MIC) and minimum bactericidal concentration (MBC) values among the bacterial isolates, which was expected of a reference antibiotic. Gram-negative strains exhibited lower sensitivity to CSP-NiO nanoparticles as compared to Gram-positive strains, as evidenced by reduced MIC and MBC levels.

Table 1 Minimum inhibitory concentration (MIC) and minimum bactericidal concentration (MBC) of cress seed mucilage polysaccharide (CSP), CSP-NiO nanoparticles, and chloramphenicol against multi-drug resistance pathogenic strains. Values are expressed as mean ± SD (n = 3), and concentrations are reported in µg/mL.

Bacteria	CSP (µg/mL)		Chloramphenicol (µg/mL)		CSP-NiO NPs (µg/mL)	
	MIC	MBC	MIC	MBC	MIC	MBC
E. coli	100 ± 0.8	100 ± 1.1	50 ± 0.6	100 ± 0.9	50 ± 0.5	100 ± 0.7
K. pneumonia	100 ± 0.7	100 ± 1.0	50 ± 0.7	100 ± 1.2	50 ± 0.6	100 ± 0.8
S. aureus	50 ± 0.5	100 ± 0.9	25 ± 0.4	50 ± 0.6	25 ± 0.3	50 ± 0.5
C. tetani	50 ± 0.6	100 ± 1.0	25 ± 0.5	50 ± 0.7	25 ± 0.4	50 ± 0.6

3.9 Growth Kinetics of Bacterial Cells Treated with Different Concentrations of CSP and CSP-NiO Nanoparticles

The representative effects of cress seed mucilage polysaccharides (CSP) and CSP-NiO nanoparticles on bacterial proliferation can be explained by the curves of bacterial growth in Fig. 9a-b. Untreated control cultures exhibited normal growth, reaching the stationary stage in about 25 hours. Figure 9a shows that CSP treatment reduced bacterial growth, especially at higher concentrations, but did not completely inhibit it. In contrast, Fig. 9b shows that CSP-NiO nanoparticles caused a stronger concentration-dependent bacterial growth inhibition. Growth was partially inhibited at 50 µg/mL, and at 100 and 200 µg/mL, it was significantly inhibited in Gram-positive (*S. aureus and C. tetani*) and Gram-negative (*E. coli*

and K. pneumoniae) species. Generally, Gram-positive strains were more susceptible than Gram-negative strains, with the strongest growth inhibition observed at 200 µg/mL CSP-NiO nanoparticles.

Figure 9a. Representative growth kinetic profiles of *S. aureus, C. tetani, E. coli*, and *K. pneumoniae* following exposure to cress seed mucilage polysaccharide (CSP) at different concentrations (0-200 µg/mL). Untreated cells (0 µg/mL) served as a control. Optical density at 600 nm (OD600) was recorded at the indicated time intervals over 25 hours.

3.10 CSP-NiO Nanoparticles Induced Reactive Oxygen Species (ROS) Generation

The intracellular reactive oxygen species (ROS) generation in the bacterial strains treated with cress seed mucilage polysaccharide (CSP) and CSP-NiO nanoparticles was quantified using DCFH-DA fluorescence assay and expressed as a percentage relative to the untreated control. As shown in Fig. 10a, CSP treatment resulted in a moderate, concentration-dependent increase in ROS levels, showing approximately 1.2 to 1.4-fold elevation compared to the untreated control. In contrast, Fig. 10b demonstrates that CSP-NiO nanoparticles caused a significantly higher elevation in ROS generation across all tested strains. At higher concentrations (100–200 µg/mL), CSP-NiO nanoparticles increased ROS levels by approximately 1.6 to 2.0-fold relative to the control. Among all the tested strains, *S. aureus* exhibited the highest ROS induction, followed by *C. tetani*, whereas *E. coli* and *K. pneumoniae* showed comparatively lower ROS generation. The results indicate that CSP-NiO nanoparticles exert an antibacterial effect through increased oxidative stress.

3.11 Effect of CSP-NiO Nanoparticles on Protein Leakage from Bacterial Cell Membranes

The effect of cress seed mucilage polysaccharide (CSP) and CSP-NiO nanoparticles on bacterial cell membrane integrity was evaluated by measuring protein leakage (Fig. 11a-b). The untreated control cells showed negligible protein release, which means that the cell membranes were intact when kept in the normal growth conditions. Triton-X caused a marked protein efflux, which revealed complete disruption of the membrane. As shown in Fig. 11a, CSP treatment had a moderate increase in the leakage of proteins, which increased in a concentration-dependent manner but was still lower than the leakage in nanoparticle-treated cells. On the other hand, Fig. 11b shows that CSP-NiO nanoparticles cause a strong, concentration-dependent increase in protein leakage in all bacterial strains tested during a 6-hour incubation. The protein efflux increased with increasing nanoparticle concentration and peaked at the highest concentration of nanoparticles. In cells treated with CSP-NiO nanoparticles, the protein leakage was measured to range between 18.96 and 38.27 µg/mL in *S. aureus*, 24.51 to 46.23 µg/mL in *C. tetani*, 15.61 to 36.61 µg/mL in *E. coli*, and 14.94 to 27.02 µg/mL in *K. pneumoniae.*

In general, Gram-positive bacteria (*S. aureus and C. tetani*) exhibited a higher level of protein leakage in comparison to Gram-negative bacteria, indicating an increased vulnerability of the membrane in CSP-NiO

nanoparticles. The high protein leakage rate observed after exposure to nanoparticles reveals that there is a severe disturbance of bacterial cell membrane integrity.

3.12 Effect of CSP-NiO Nanoparticles on Genomic DNA Integrity

The integrity of bacterial genomic DNA following treatment with CSP and CSP-NiO nanoparticles was assessed using agarose gel electrophoresis (Fig. 12). The untreated cells used as a negative control exhibited an intact DNA band with no visible smearing, indicating preserved genomic integrity. CSP-treated DNA displayed a gradual decrease in band intensity with increasing concentration, accompanied by mild smearing, suggesting concentration-dependent DNA damage. In contrast, CSP-NiO nanoparticles-treated DNA showed weak DNA bands with extensive smearing, particularly at higher concentrations, implying the disruption of genomic DNA integrity. Overall, CSP-NiO nanoparticles induced stronger DNA damage than CSP, supporting their enhanced antibacterial potential.

4. Discussion

The development of green-synthesized metal oxide nanoparticles has gained significant interest due to their environmentally friendly, cost-effective, and sustainable production routes that avoid the use of hazardous chemicals [37]. However, conventional chemical and physical synthesis methods often involve toxic precursors that can compromise the biocompatibility [38]. The usage of metal oxide nanoparticles in therapeutic use remains an obstacle [39]. Though the development in nanoparticle research has addressed many such applications and enhanced conditions for their use in therapeutics [40]. Current studies have shown that nanoparticles, being smaller in size, exhibit greater antimicrobial activity against various infectious microorganisms [41]. Nickel oxide nanoparticles, having physico-chemical properties such as supercapacitance, electron transfer ability, high chemical stability, and electrocatalysis, have gained the interest of many research groups for different therapeutic potential [42]. The present study addresses this challenge by utilizing *Lepidium sativum* (cress) seed mucilage polysaccharide (CSP) as a natural reducing and stabilizing agent for the green synthesis of NiO nanoparticles. Polysaccharides, with their abundant hydroxyl groups, play a critical role in stabilizing metal ions during nanoparticle synthesis, as confirmed in earlier studies [43, 44]. In this context, many research groups have proposed that Nickel oxide nanoparticles have potential as an antitumor agent and antimicrobial agent [41, 45]. Although the particular mechanism behind the antimicrobial potential of Nickel oxide nanoparticles has not been discovered yet. While many mechanisms of antimicrobial potential, such as the generation of ROS, the release of metal ions, cell wall damage, and the propagation of the cell envelope, have been stated for many metal oxide nanoparticles against several Gram-positive and Gram-negative bacteria, the mechanism remains largely unexplored and needs extensive evaluation for the safe use of nanoparticles as modern antimicrobial agents. In this study, we explored the mechanism to understand the antimicrobial activity of CSP-NiO nanoparticles against Gram-positive (*S. aureus* and *C. tetani*) and Gram-negative (*E coli* and *K. pneumoniae*) bacteria using different antimicrobial assays.

The stable formation of CSP-NiO NPs was authenticated through numerous characterization methods, such as UV-visible spectroscopy, FTIR, SEM, XRD, and EDX, elucidating a structural integrity and stability. The UV-visible analysis exhibited an absorbance peak at 350 nm, characteristic of NiO NPs aligned with previous reports [46]. The FTIR spectra revealed strong Ni-O vibrations at ~ 570 cm^{-1} along with polysaccharide-associated functional groups, confirming the role of CSP in surface modification and stabilization [47]. The XRD analysis validated the cubic crystalline phase with diffraction peaks matching standard NiO planes, further confirming successful nanoparticle formation [48]. SEM analysis revealed irregular agglomerated nanoscale clusters typical of green-synthesized metal oxides, whereas the EDX confirmed the elemental purity, with Ni and O being predominant [49]. The biocompatibility of CSP-NiO NPs was tested on the freshly obtained HRBCs to ensure their biosafety. As per American society, the biological substances exhibiting a percent hemolysis higher than 5% is characterized as hemolytic, ranging from 2% to 5% are minimally hemolytic, whereas less than 2% is non-hemolytic [37]. Regarding this, our results showed that the CSP-NiO nanoparticles are non-toxic at the lower concentration (25 µg/mL) with 1.12 ± 0.31% hemolysis, whereas the higher hemolysis of 5.02 ± 0.89% was recorded at 200 µg/mL, which falls within a slightly hemolytic range. These results are in agreement with the prior studies that assessed the biological compatibility of green-synthesized NiO NPs tested on the freshly extracted HRBCs and macrophages, indicating that they were non-toxic even at lower doses [50, 51].

The disc diffusion assay demonstrated that CSP-NiO nanoparticles inhibited bacterial growth dose-dependently with maximum activity at 200 µg/mL, which was higher than CSP alone. This enhanced activity suggests the synergetic effect of NiO NPs, likely associated with the release of nickel ions from CSP-NiO nanoparticles that increased membrane permeability and ROS generation, leading to cell death. These results are in agreement with a previous study that reported the green synthesis of NiO nanoparticles as antimicrobial agents [52, 53]. The identified MIC and MBC values also support the antibacterial activity of CSP-NiO nanoparticles by showing a stronger susceptibility of Gram-positive strains (*S. aureus, C. tetani*). This selectivity could be explained by differences in membrane polarity. Gram-positive bacteria have a higher cationic charge when compared to Gram-negative bacteria. This promotes the enhanced permeability of negatively charged free radicals, thus promoting more cellular destruction [54]. Another possible cause can be the structural complexities of the gram-negative bacterial cell wall. Gram-positive bacteria have a dense, multilayered peptidoglycan cell wall that surrounds cytoplasmic membranes, and the gram-negative cell wall consists of a thin peptidoglycan shell with an outer lipid bilayer, which is rich in lipopolysaccharides. In gram-negative bacteria, the outer lipid bilayer is considered a barrier that limits the cell uptake of reactive oxygen species [55]. Similar results are obtained with green-synthesized NiO and CuO nanoparticles, in which surface charge and smaller particle size contribute to the higher antimicrobial activity [56]. The growth kinetics of the bacteria further explained the inhibitory effect of CSP-NiO nanoparticles. The growth kinetic study showed a clear, dose-dependent inhibition, where CSP-NiO nanoparticles significantly inhibited bacterial growth compared to CSP and control. It is important to note that there was considerable suppression at 200 µg/mL. The fast growth inhibition of bacteria at a concentration of 200 µg mL of CSP-NiO nanoparticles compared to 100 and 50 µg mL is due to the availability of a limited amount of nickel ions.

The current growth inhibition at this concentration is aligned with earlier findings regarding green-synthesized NiO nanoparticles synthesized using *Aloe vera* and *Ocimum sanctum*, in which the nanoparticles inhibited metabolic activity and delayed the progression of the cell cycle [57, 58].

The improved antibacterial effect of CSP-NiO nanoparticles is mechanistically explained by various synergistic interactions. Quantitative ROS assays indicated that exposure to CSP-NiO nanoparticles caused a substantial level of intracellular oxidative stress, and the generation of ROS was up to two-fold relative to untreated controls. The observation is aligned with the known mechanism according to which NiO nanoparticles catalyze the generation of hydroxyl (-OH) and superoxide (O_2-) radicals, which in turn can oxidize cellular macromolecules and disrupt redox balance [59] High levels of ROS enhance lipid peroxidation and membrane disorganization, which is observed by leakage of more protein out of CSP-NiO-treated cells. This leakage is a characteristic of impaired membrane integrity and is consistent with previous publications that have implicated oxidative destabilization of the membrane as a result of nanoparticle-induced bacteriolysis [60]. Moreover, agarose gel electrophoresis revealed DNA fragmentation and smearing in CSP-NiO-treated cells, which indicates direct genotoxic effects probably caused by oxidative damage. The use of NiO and ZnO nanoparticles has also been shown to cause similar degradation of DNA in *Escherichia coli*, thus supporting the role of oxidative stress and electrostatic interactions between Ni^{2+} ions and bacterial DNA as a key antibacterial process [61].

Conclusion

The present study demonstrates the easy and non-toxic synthesis of nickel oxide nanoparticles (NiO NPs) utilizing polysaccharides derived from seeds of *Lepidium sativum*, thereby affirming their stable structure and multifunctional attributes. This green synthesis resulted in crystalline, surface-stabilized NiO nanoparticles exhibiting potent antibacterial activity and negligible hemolytic effects, even at elevated doses. The CSP-NiO nanoparticles exhibited a strong, dose-dependent antimicrobial activity against Gram-positive and Gram-negative bacteria. Mechanistic investigations revealed that this bactericidal action is largely triggered by oxidative stress caused by reactive oxygen species, leading to membrane injury, protein release, and degradation of genomic DNA, which ultimately induces bacterial cell death, with Gram-positive strains showing greater sensitivity. These results demonstrate the usefulness of cress-seed mucilage polysaccharide as a biomatrix in nanomaterials synthesis and emphasize the potency of CSP-NiO nanoparticles as a safe and effective antimicrobial agent.

Declarations

Competing interests:

The authors declare that they have no conflict of interest.

Ethics approval and consent to participate:

This article does not contain any studies with human participants or animals performed by any of the authors.

Consent for publication:

All the authors agreed and approve the paper for publication.

Funding:

This research work was supported by the Higher Education Department, Government of Khyber Pakhtunkhwa, under the Higher Education Research Endowment Fund (HEREF), Project No. 3111, and the Higher Education Commission of Pakistan, Project No. NRPU-10569.

Author Contribution

Y.J., M.A., S.A., A.A: methodology, data collection, original data analysis, writing original draft; A.A: supervision, A.A., and S.A: data presentation, writing and editing of manuscript; D.L: data collection, software; A.F.A, S.A., and A.A: validation, software, visualization, resources, writing original draft, funding acquisition and revision of the manuscript. All authors have read and agreed to the published version of the manuscript.

Acknowledgement

We are very thankful to the Ongoing Research Funding program, (ORF-2025-218), King Saud University, Riyadh, Saudi Arabia.

Data Availability

The datasets used and analyzed during the current study available from the corresponding author on reasonable request.

References

1. Puri, B., Vaishya, R. & Vaish, A. Antimicrobial resistance: Current challenges and future directions. *Med. J. Armed Forces India*. **81**, 247–258 (2025).
2. Nazir, A. et al. The global challenge of antimicrobial resistance: mechanisms, case studies, and mitigation approaches. *Health Sci. Rep.* **8**, e71077 (2025).

3. Auzin, A. et al. What is the evidence base of used aggregated antibiotic resistance percentages to change empirical antibiotic treatment? A scoping review. *Clin. Microbiol.* **28**, 928–935 (2022).
4. Tarin-Pello, A., Suay-Garcia, B. & Perez-Gracia, M. T. Antibiotic resistant bacteria: current situation and treatment options to accelerate the development of a new antimicrobial arsenal. *Expert Rev. anti-infective therapy*. **20**, 1095–1108 (2022).
5. Sharmin, S. et al. Nanoparticles as antimicrobial and antiviral agents: A literature-based perspective study. *Heliyon 7*. (2021).
6. Tijani, N. A. et al. Metallic nanoparticles: a promising novel therapeutic tool against antimicrobial resistance and spread of superbugs. *BioMetals 38*, 55–88. (2025).
7. Do, H. T. T. et al. T.T.H. Advances in silver nanoparticles: unraveling biological activities, mechanisms of action, and toxicity. *Appl. Nanosci.* **15**, 1 (2025).
8. Rani, L. & Chauhan, R. Transition metal (Mn-, Ni-, Co-and Cu-) doped ZnS nano-flowers for morphological, structural, optical, elemental and antibacterial studies. *Transition Metal Chemistry* 1–20. (2025).
9. Brown, C. D., Cruz, D. M., Roy, A. K. & Webster, T. Synthesis and characterization of PVP-coated tellurium nanorods and their antibacterial and anticancer properties. *J. Nanopart. Res.* **20**, 254 (2018).
10. Khan, A., Vishvakarma, R., Sharma, P., Sharma, S. & Vimal, A. Green Synthesis of Metal-Oxide Nanoparticles from Fruits and Their Waste Materials for Diverse Applications. In *Nanomaterials from Agricultural and Horticultural Products*; Springer: ; pp. 81–119. (2023).
11. Jaji, N. D. et al. Advanced nickel nanoparticles technology: From synthesis to applications. *Nanatechnol. reviews*. **9**, 1456–1480 (2020).
12. Iqbal, S., Jabeen, F., Chaudhry, A. S., Shah, M. A. & Batiha, G. E. S. Toxicity assessment of metallic nickel nanoparticles in various biological models: An interplay of reactive oxygen species, oxidative stress, and apoptosis. *Toxicol. Industrial Health*. **37**, 635–651 (2021).
13. Huynh, K. G., Tran, K., Le, Q. N. & Doan, L. Surface Modifications of Zinc Oxide, Copper Oxide, and Nickel Oxide Particles with Chitosan, Poly (ethylene glycol), Poly (vinyl alcohol), and Poly (vinylpyrrolidone) as Antimicrobial Agents against Staphylococcus aureus, Pseudomonas aeruginosa, and Salmonella enterica. *ACS omega*. **10**, 51962–51984 (2025).
14. Behera, N. et al. Oxidative stress generated at nickel oxide nanoparticle interface results in bacterial membrane damage leading to cell death. *RSC Adv.* **9**, 24888–24894 (2019).
15. Terreni, M., Taccani, M. & Pregnolato, M. New antibiotics for multidrug-resistant bacterial strains: latest research developments and future perspectives. *Molecules* **26**, 2671 (2021).
16. Kumar, J. A. et al. A focus to green synthesis of metal/metal based oxide nanoparticles: Various mechanisms and applications towards ecological approach. *J. Clean. Prod.* **324**, 129198 (2021).
17. Seth, R. & Meena, A. Enzymes-based nanomaterial synthesis: an eco-friendly and green synthesis approach. *Clean. Technol. Environ. Policy*. **27**, 5775–5798 (2025).

18. Khan, S. A. et al. Phytomolecules-coated NiO nanoparticles synthesis using abutilon indicum leaf extract: antioxidant, antibacterial, and anticancer activities. *International J. Nanomedicine* 1757–1773. (2021).
19. Plucinski, A., Lyu, Z. & Schmidt, B. V. Polysaccharide nanoparticles: from fabrication to applications. *J. Mater. Chem. B*. **9**, 7030–7062 (2021).
20. Liu, J., Willför, S. & Xu, C. A review of bioactive plant polysaccharides: Biological activities, functionalization, and biomedical applications. *Bioactive carbohydrates Diet. fibre*. **5**, 31–61 (2015).
21. Sidhu, A. K., Verma, N. & Kaushal, P. Role of biogenic capping agents in the synthesis of metallic nanoparticles and evaluation of their therapeutic potential. *Front. Nanatechnol.* **3**, 801620 (2022).
22. Gupta, S. & Gupta, R. Research update on the therapeutic potential of garden cress (Lepidium sativum Linn.) with threatened status. *Curr. Drug Res. Reviews Formerly: Curr. Drug Abuse Reviews*. **16**, 369–380 (2024).
23. Shiam, M. A. H., Islam, M. S., Ahmad, I. & Haque, S. S. A review of plant-derived gums and mucilages: Structural chemistry, film forming properties and application. *J. Plast. Film Sheeting*. **41**, 195–237 (2025).
24. Khan, I. U. et al. Pichia pastoris Mediated Digestion of Water-Soluble Polysaccharides from Cress Seed Mucilage Produces Potent Antidiabetic Oligosaccharides. *Pharmaceuticals* **17**, 704 (2024).
25. Khan, I. U. et al. Anti-oxidative and anti-apoptotic oligosaccharides from pichia pastoris-fermented cress polysaccharides ameliorate chromium-induced liver toxicity. *Pharmaceuticals* **17**, 958 (2024).
26. Khan, I. U. et al. Unlocking the in vitro and in vivo antioxidant and anti-inflammatory activities of polysaccharide fractions from Lepidium sativum seed-coat mucilage. *Heliyon 10*. (2024).
27. Shiehnezhad, M., Zarringhalami, S. & Malekjani, N. Optimization of Microwave-Assisted Extraction of Mucilage from Ocimum basilicum var. album (L.) Seed. *Journal of Food Processing Preservation 2023*, 5524621. (2023).
28. Xiaolong, J., Jianhang, G., Jingyuan, T., Ke, M. & Yanqi, L. Research progress on degradation methods and product properties of plant polysaccharides. *Journal Light Industry* **38**. (2023).
29. Mirsalari, F., Tahanpesar, E. & Sanaeishoar, H. Biosynthesis of NiO-NPs using mucilage of Cordia myxa fruit and their potential application as an efficient catalyst for the synthesis of chromenes. *Res. Chem. Intermed.* **49**, 4127–4148 (2023).
30. Singh, A. et al. Structurally and morphologically engineered single-pot biogenic synthesis of NiO nanoparticles with enhanced photocatalytic and antimicrobial activities. *J. Clean. Prod.* **343**, 131026 (2022).
31. Güler, Ş. et al. Evaluation of antibacterial efficacy of Lawsonia inermis Linn (henna) on periodontal pathogens using agar well diffusion and broth microdilution methods: an in-vitro study. *BioMedicine* **13**, 25 (2023).
32. Rahman, A. et al. Facile Synthesis and Application of Ag-NPs for Controlling Antibiotic-ResistantPseudomonas spp. and Bacillus spp. in a Poultry Farm Environment. *Journal of Nanotechnology 2023*, 6260066. (2023).

33. Sondi, I. & Salopek-Sondi, B. Silver nanoparticles as antimicrobial agent: a case study on E. coli as a model for Gram-negative bacteria. *J. colloid interface Sci.* **275**, 177–182 (2004).
34. Ogami, A. et al. Pathological features of different sizes of nickel oxide following intratracheal instillation in rats. *Inhalation Toxicol.* **21**, 812–818 (2009).
35. Sahoo, B., Panigrahi, L. L., Jena, S., Jha, S. & Arakha, M. Oxidative stress generated due to photocatalytic activity of biosynthesized selenium nanoparticles triggers cytoplasmic leakage leading to bacterial cell death. *RSC Adv.* **13**, 11406–11414 (2023).
36. Yılmaz, H., Kalefetoğlu Macar, T., Macar, O., Çavuşoğlu, K. & Yalçın, E. DNA fragmentation, chromosomal aberrations, and multi-toxic effects induced by nickel and the modulation of Ni-induced damage by pomegranate seed extract in Allium cepa L. *Environ. Sci. Pollution Res.* **30**, 110826–110840 (2023).
37. Radulescu, D. M. et al. Green synthesis of metal and metal oxide nanoparticles: a review of the principles and biomedical applications. *Int. J. Mol. Sci.* **24**, 15397 (2023).
38. Kirubakaran, D. et al. A comprehensive review on the green synthesis of nanoparticles: advancements in biomedical and environmental applications. *Biomedical Mater. Devices*. **4**, 388–413 (2026).
39. Negrescu, A. M. et al. Metal oxide nanoparticles: review of synthesis, characterization and biological effects. *J. Funct. Biomaterials*. **13**, 274 (2022).
40. Malik, S., Muhammad, K. & Waheed, Y. Emerging applications of nanotechnology in healthcare and medicine. *Molecules* **28**, 6624 (2023).
41. Skłodowski, K. et al. Metallic nanosystems in the development of antimicrobial strategies with high antimicrobial activity and high biocompatibility. *Int. J. Mol. Sci.* **24**, 2104 (2023).
42. Arulkumar, E., Shree, S. S. & Thanikaikarasan, S. Structure, morphology, composition, optical properties of CuO/NiO nanocomposite for electrochemical energy storage devices. *Results Chem.* **6**, 101087 (2023).
43. Bilal, M., Gul, I., Basharat, A. & Qamar, S. A. Polysaccharides-based bio-nanostructures and their potential food applications. *Int. J. Biol. Macromol.* **176**, 540–557 (2021).
44. Maind, R. et al. Nickel Oxide Based Nanoparticles: Green Synthesis, Morphological Assessment, and Their Biological Properties. *Universal J. Green. Chemistry* 229–254. (2024).
45. Talib, W. H. et al. Natural Products and Altered Metabolism in Cancer: Therapeutic Targets and Mechanisms of Action. *Int. J. Mol. Sci.* **25**, 9593 (2024).
46. Iqbal, J. et al. Green synthesis and characterizations of Nickel oxide nanoparticles using leaf extract of Rhamnus virgata and their potential biological applications. *Appl. Organomet. Chem.* **33**, e4950 (2019).
47. Al-Zaqri, N., Umamakeshvari, K., Mohana, V., Muthuvel, A. & Boshaala, A. Green synthesis of nickel oxide nanoparticles and its photocatalytic degradation and antibacterial activity. *J. Mater. Sci.: Mater. Electron.* **33**, 11864–11880 (2022).

48. Haider, A. J., Al-Anbari, R., Sami, H. M. & Haider, M. J. Photocatalytic activity of nickel oxide. *J. Mater. Res. Technol.* **8**, 2802–2808 (2019).
49. Hafeez, M. et al. Green synthesis of nickel oxide nanoparticles using populus ciliata leaves extract and their potential antibacterial applications. *S. Afr. J. Chem.* **75**, 168–173 (2021).
50. Nayal, R., Mejjo, D. & Abajy, M. Y. Anti inflammatory properties and safety of green synthesized metal and metal oxide nanoparticles: a review article. *Eur. J. Med. Chem. Rep.* **11**, 100169 (2024).
51. Sabouri, Z., Akbari, A., Hosseini, H. A., Khatami, M. & Darroudi, M. Green-based bio-synthesis of nickel oxide nanoparticles in Arabic gum and examination of their cytotoxicity, photocatalytic and antibacterial effects. *Green. Chem. Lett. Reviews*. **14**, 404–414 (2021).
52. Uddin, S. et al. Green synthesis of nickel oxide nanoparticles using leaf extract of Berberis balochistanica: Characterization, and diverse biological applications. *Microscopy Res. Technique*. **84**, 2004–2016 (2021).
53. Zhang, L. et al. Ten-gram-scale mechanochemical synthesis of ternary lanthanum coordination polymers for antibacterial and antitumor activities. *Front. Chem.* **10**, 898324 (2022).
54. Berhe, M. G. & Gebreslassie, Y. T. Biomedical applications of biosynthesized nickel oxide nanoparticles. *International J. nanomedicine* 4229–4251. (2023).
55. Yin, X. et al. Multiple bacteria recognition mechanisms and their applications. *Coord. Chem. Rev.* **517**, 216025 (2024).
56. preet Singh, G., Singh, K., Chandel, K., Kaur, P. & Kaur, J. Green synthesis of NiO doped CuO nanoparticles: Potential for environmental remediation. *Inorg. Chem. Commun.* **157**, 111250 (2023).
57. Ahmad, B. et al. Green synthesis of NiO nanoparticles using Aloe vera gel extract and evaluation of antimicrobial activity. *Mater. Chem. Phys.* **288**, 126363 (2022).
58. Patil, O. P., Raja, T., Dhanraj, G. & Prabhalakshmi, K. Green Synthesis and Characterization of Zinc Oxide Nanoparticles Derived from Ocimum Sanctum Leaves: Antibacterial, Antibiofilm, and Thermal Studies. *J. Bio-and Tribo-Corrosion*. **12**, 34 (2026).
59. Cao, J. et al. Mechanistic insight on nanomaterial-induced reactive oxygen species formation. *J. Environ. Sci.* **151**, 200–210 (2025).
60. Modi, S. K., Gaur, S., Sengupta, M. & Singh, M. S. Mechanistic insights into nanoparticle surface-bacterial membrane interactions in overcoming antibiotic resistance. *Front. Microbiol.* **14**, 1135579 (2023).
61. Aslinjensipriya, A., Ragu, R., Grace Infantiya, S. & Jerome Das, S. Revealing the Substitution of Zn2 + on Nano-Structural, Magneto-Electrical, Antibacterial and Antifungal Attributes of Nickel Oxide Nanoparticles via Sol-Gel Strategy. (2022).

Figures

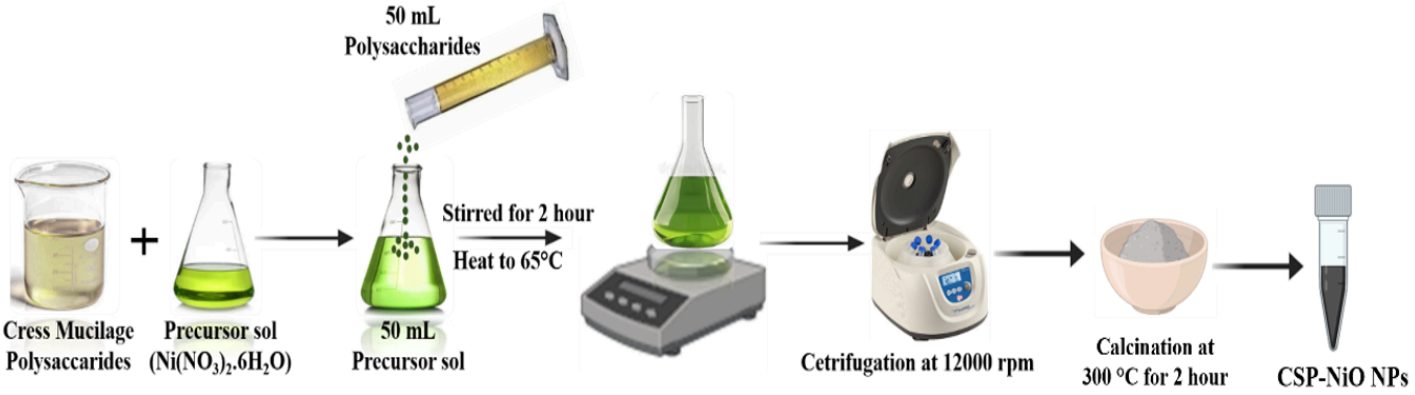

Figure 1

Flowchart representing the green synthesis of NiO nanoparticles using Cress mucilage polysaccharides.

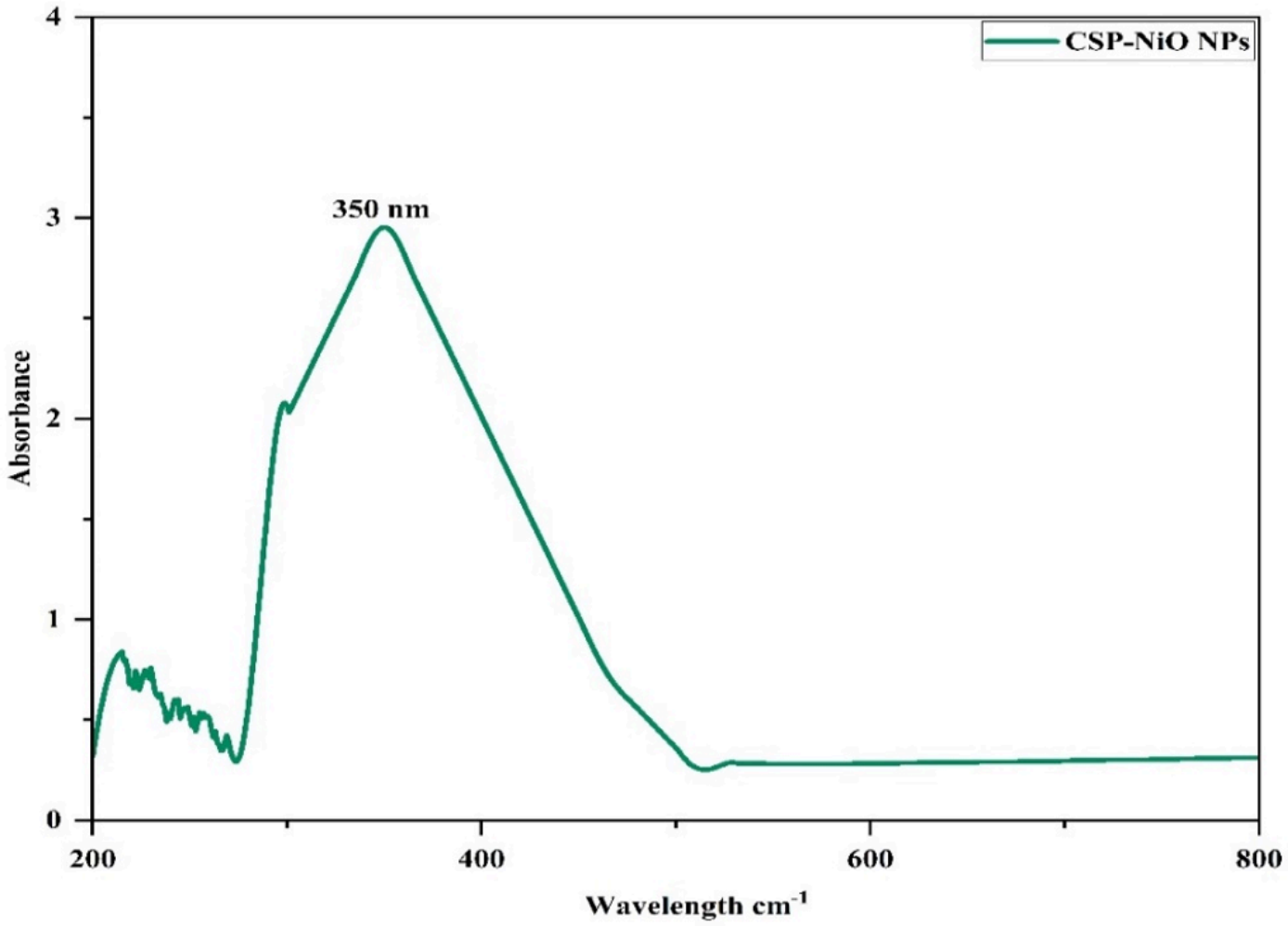

Figure 2

The ultraviolet (UV) absorption spectrum of CSP-NiO nanoparticles.

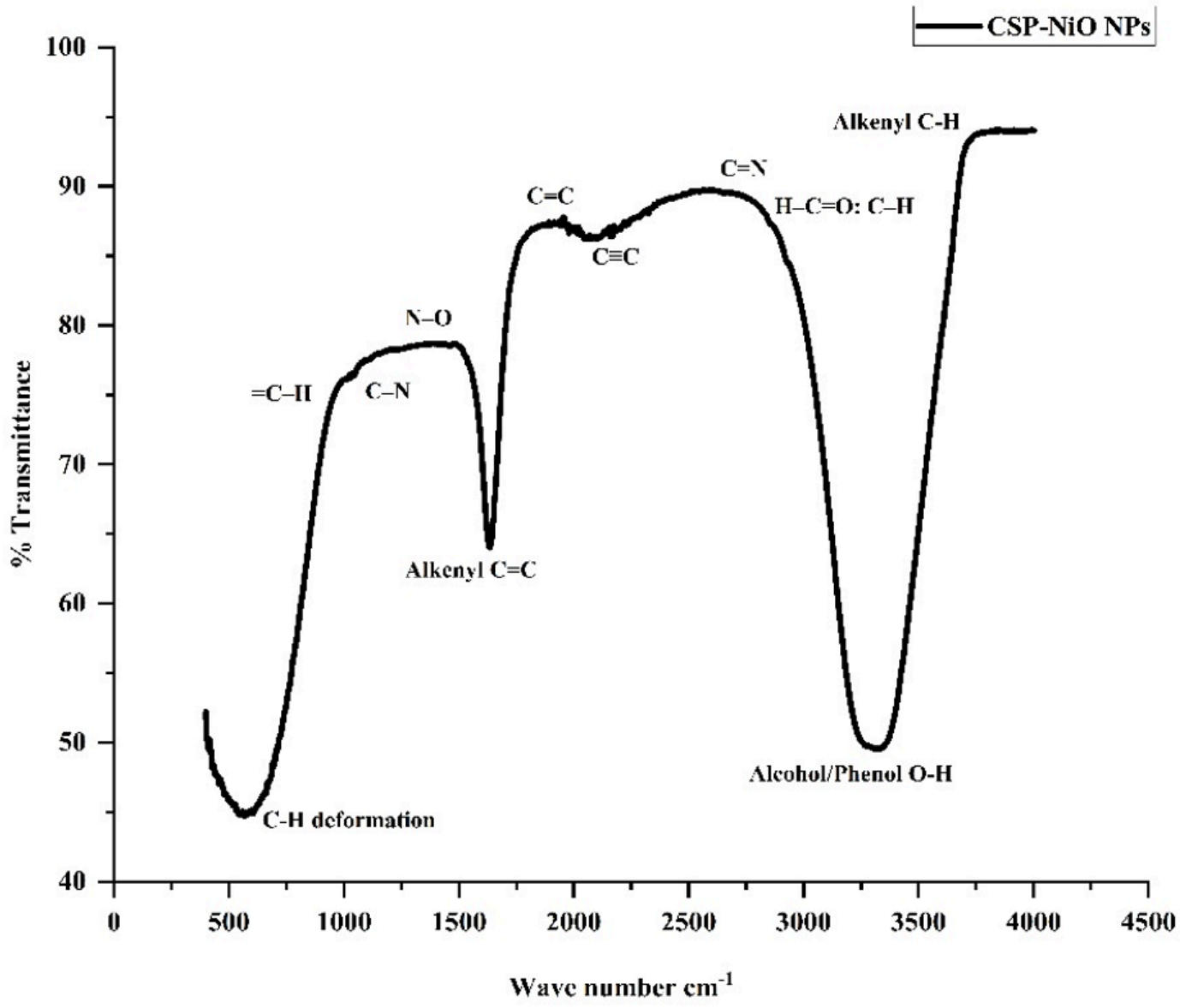

Figure 3

FTIR spectroscopic analysis of CSP-NiO NPs.

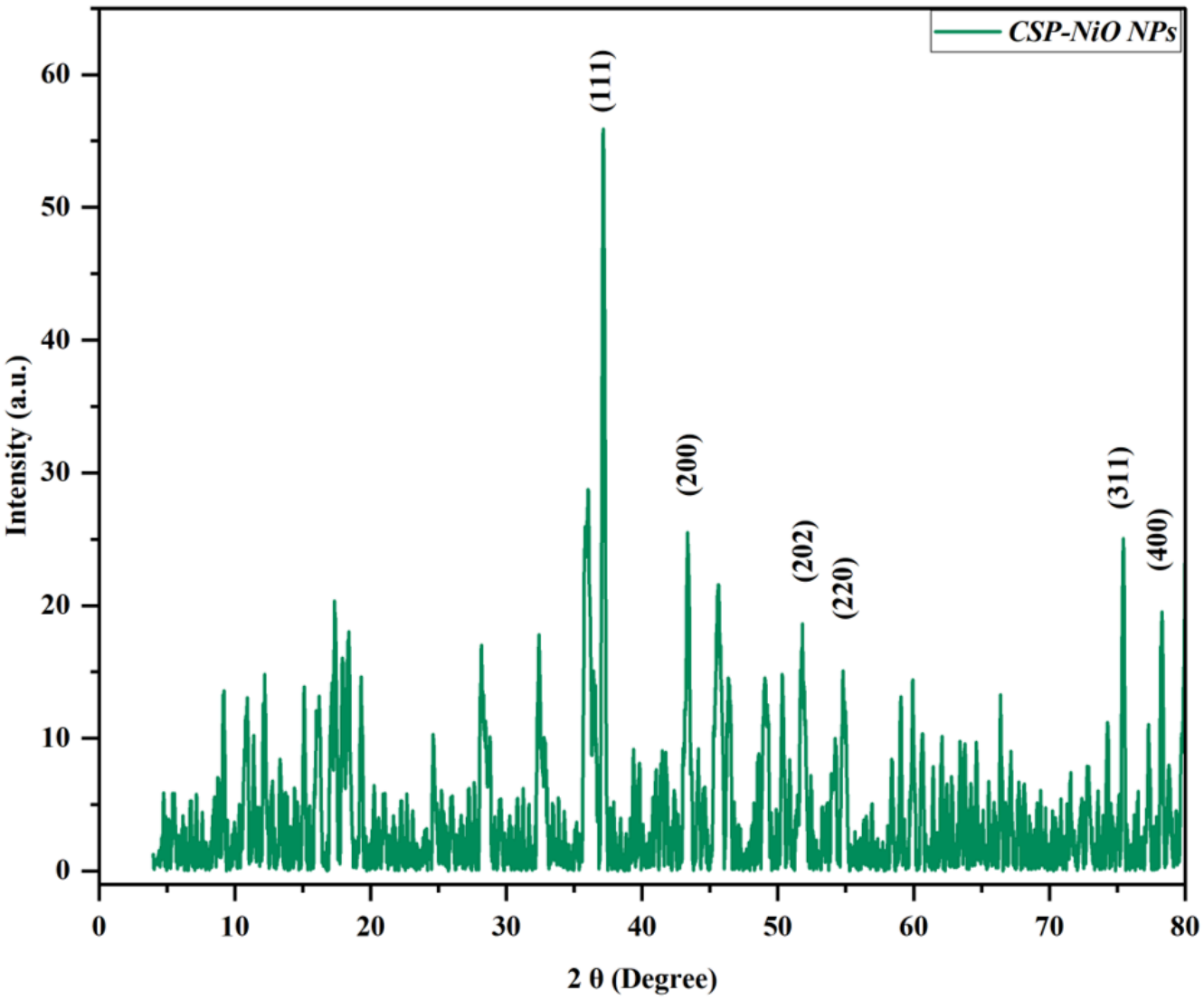

Figure 4

XRD pattern of CSP-NiO NPs.

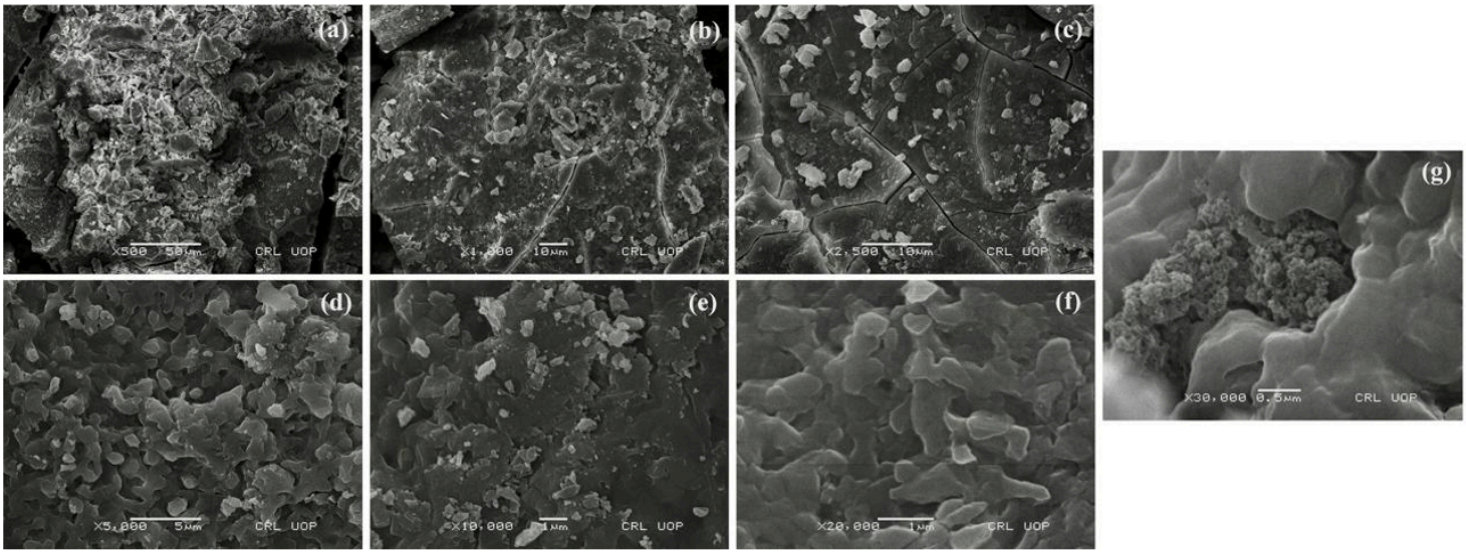

Figure 5

SEM micrographs of CSP-NiO nanoparticles recorded at increasing magnifications. (a) ×500, (b) ×1,000 (c) ×2,500 (d) ×5,000 (e) ×10,000 (f) ×20,000 (g) ×30,000.

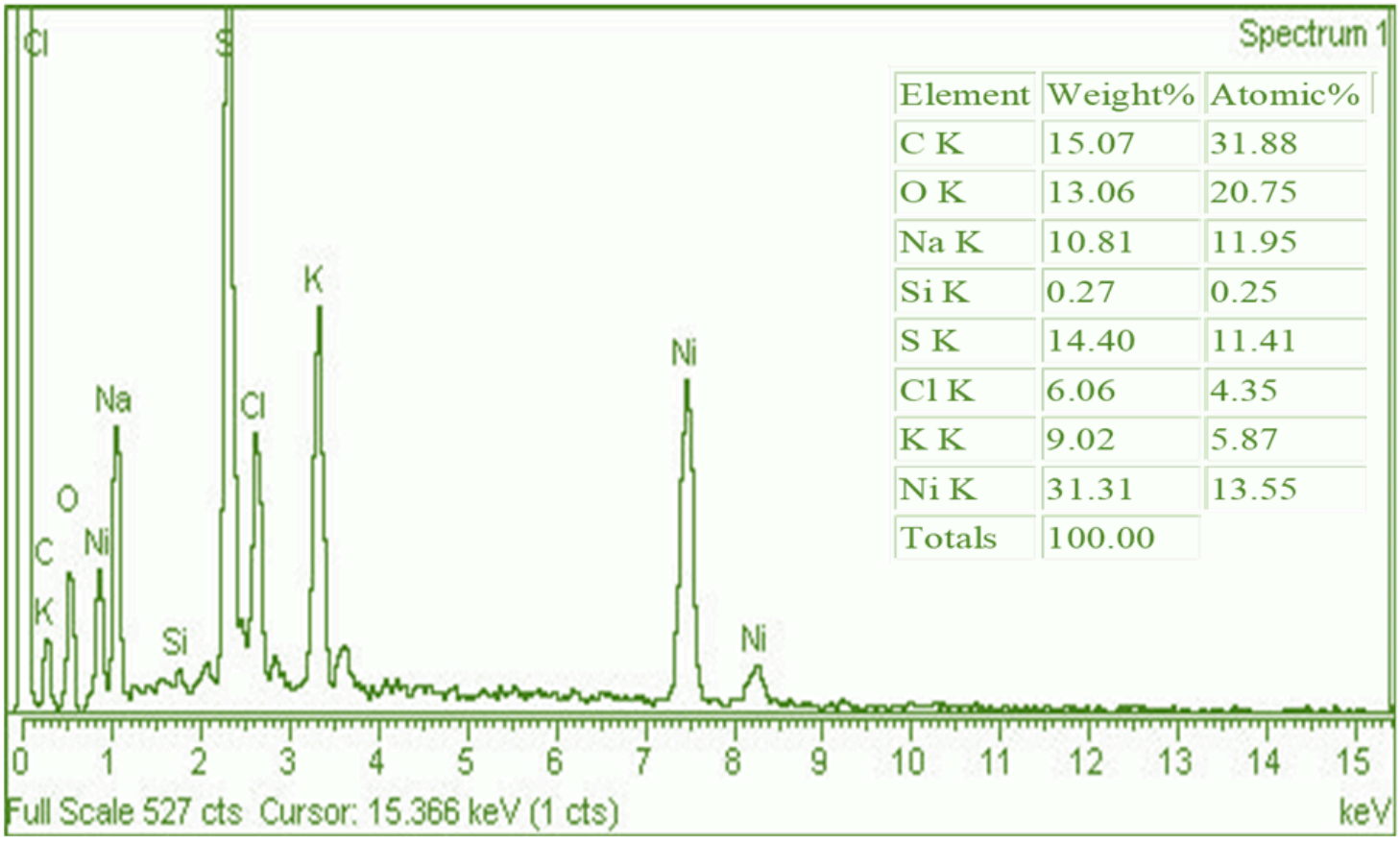

Element	Weight%	Atomic%
C K	15.07	31.88
O K	13.06	20.75
Na K	10.81	11.95
Si K	0.27	0.25
S K	14.40	11.41
Cl K	6.06	4.35
K K	9.02	5.87
Ni K	31.31	13.55
Totals	100.00	

Figure 6

Elemental composition of CSP-NiO NPs using EDX.

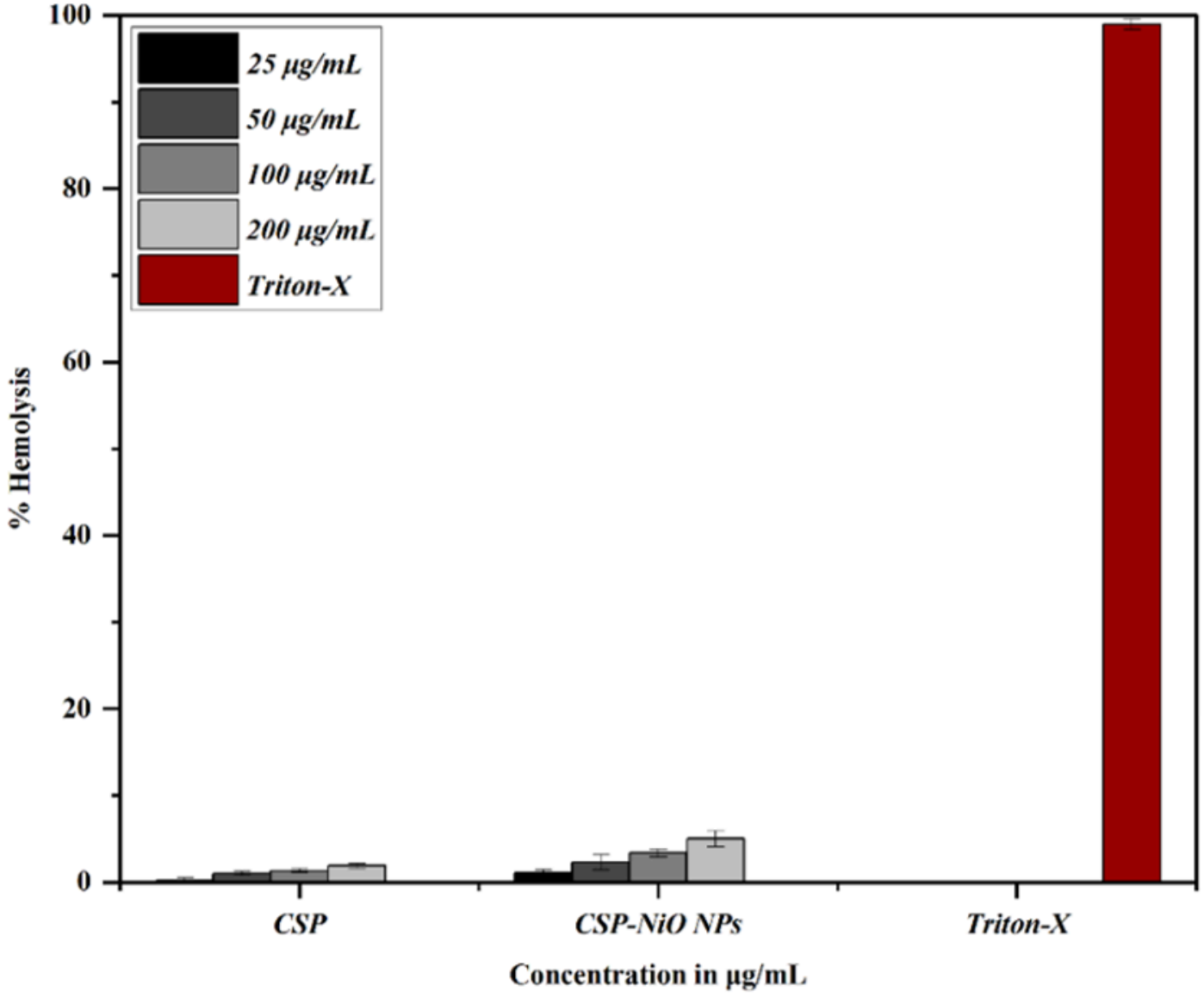

Figure 7

Percent hemolysis against human red blood cells (HRBCs) by Cress polysaccharides (CSP) and Nickel oxide nanoparticles (CSP-NiO NPs) at various screening concentrations (25-200 µg/mL) with Triton-X (0.5%) served as a positive control.

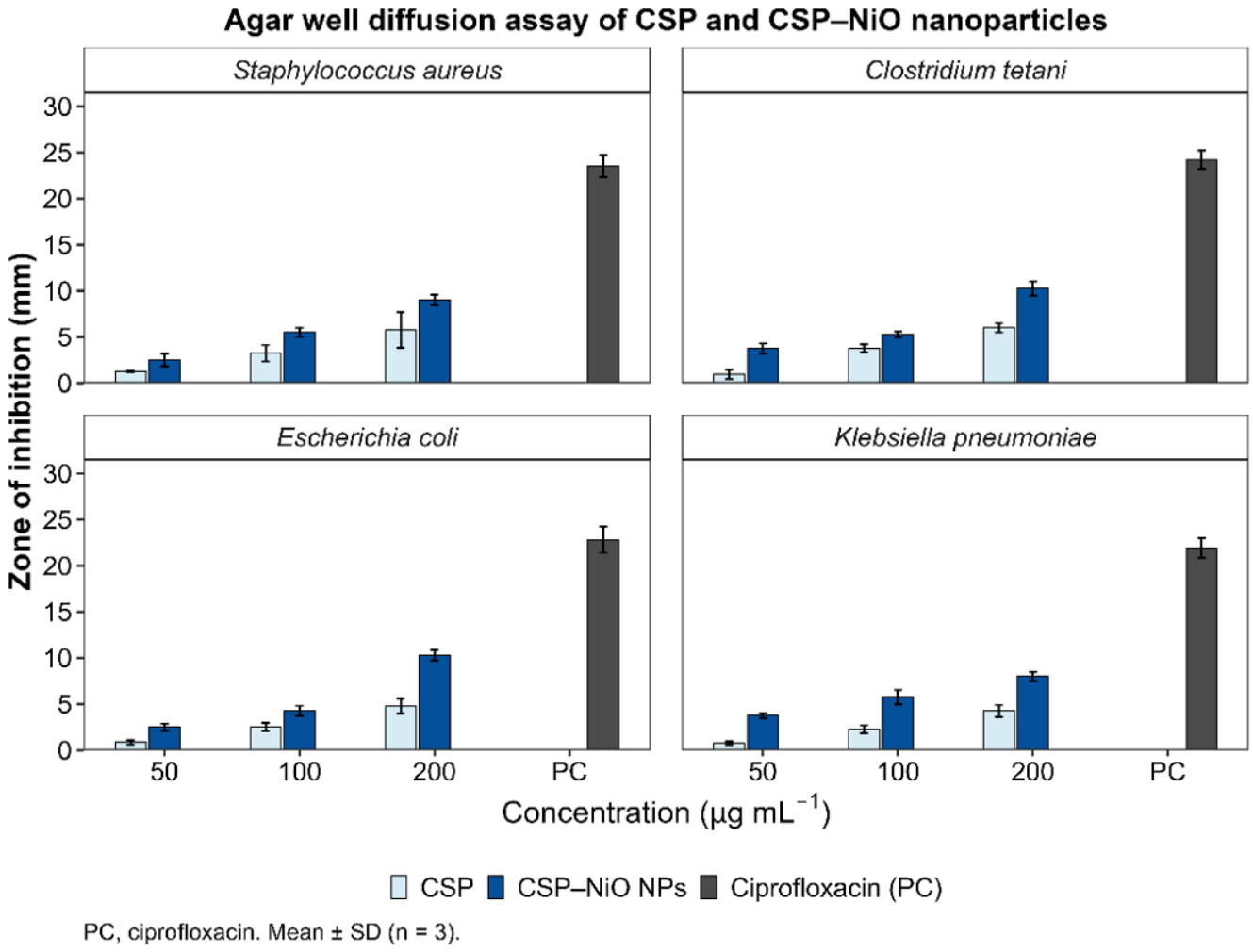

PC, ciprofloxacin. Mean ± SD (n = 3).

Figure 8

Agar well diffusion assay showing the antibacterial activity of CSP and CSP-NiO nanoparticles against *S. aureus, C. tetani, E. coli*, and *K. pneumoniae*. Zone of inhibition was measured at 50, 100, 200 µg/mL^{-1}. Ciprofloxacin (PC) served as a positive control. Data are presented as mean ± SD (n = 3).

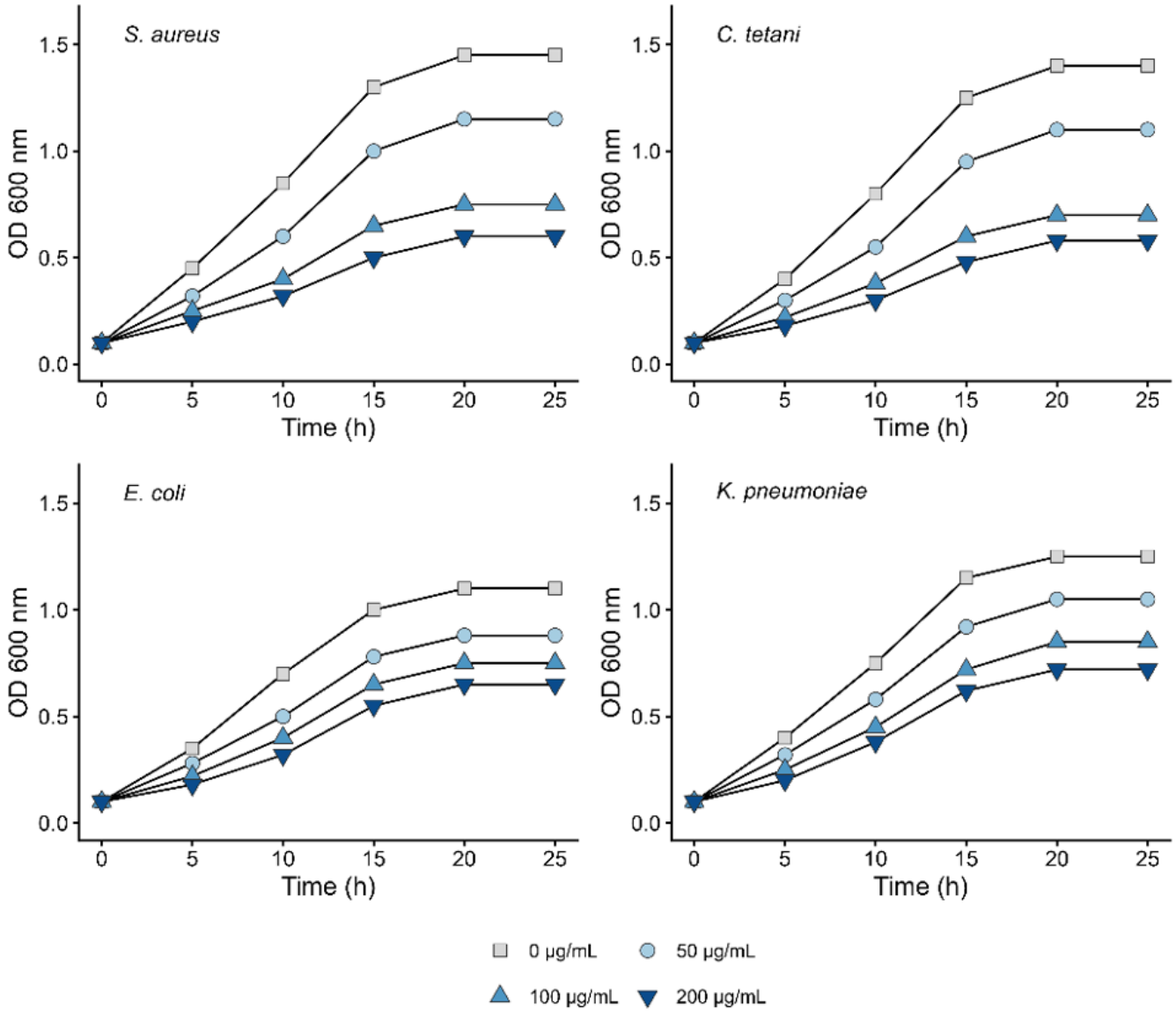

Figure 9

Figure 9a. Representative growth kinetic profiles of *S. aureus, C. tetani, E. coli*, and *K. pneumoniae* following exposure to cress seed mucilage polysaccharide (CSP) at different concentrations (0-200 µg/mL). Untreated cells (0 µg/mL) served as a control. Optical density at 600 nm (OD600) was recorded at the indicated time intervals over 25 hours.

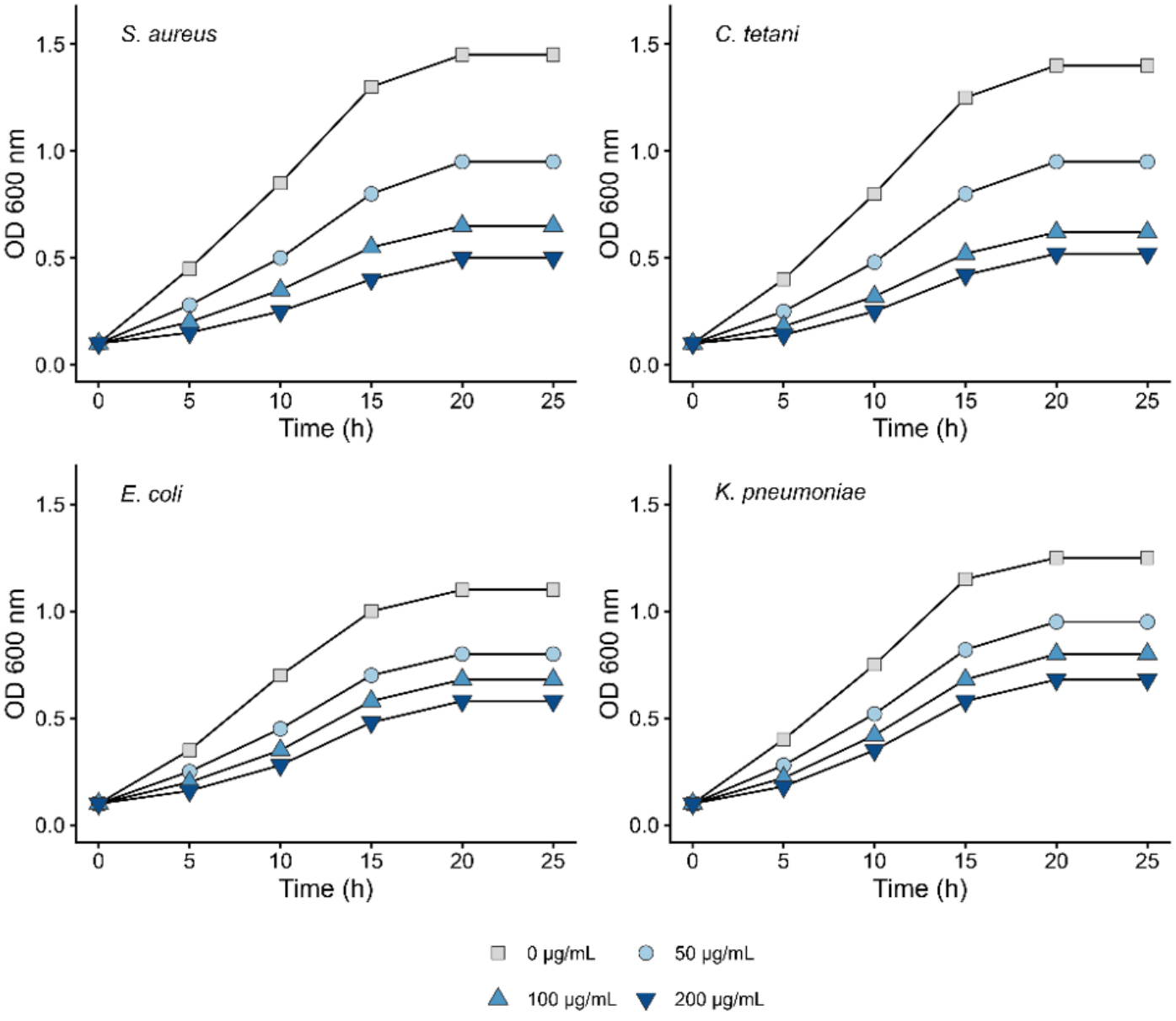

Figure 10

Figure 9b. Representative growth kinetic profiles of *S. aureus, C. tetani, E. coli*, and *K. pneumoniae* following treatment with CSP-NiO nanoparticles at different concentrations (0-200 µg/mL). Untreated cells (0 µg/mL) served as a control. Optical density at 600 nm (OD600) was recorded at the indicated time intervals over 25 hours.

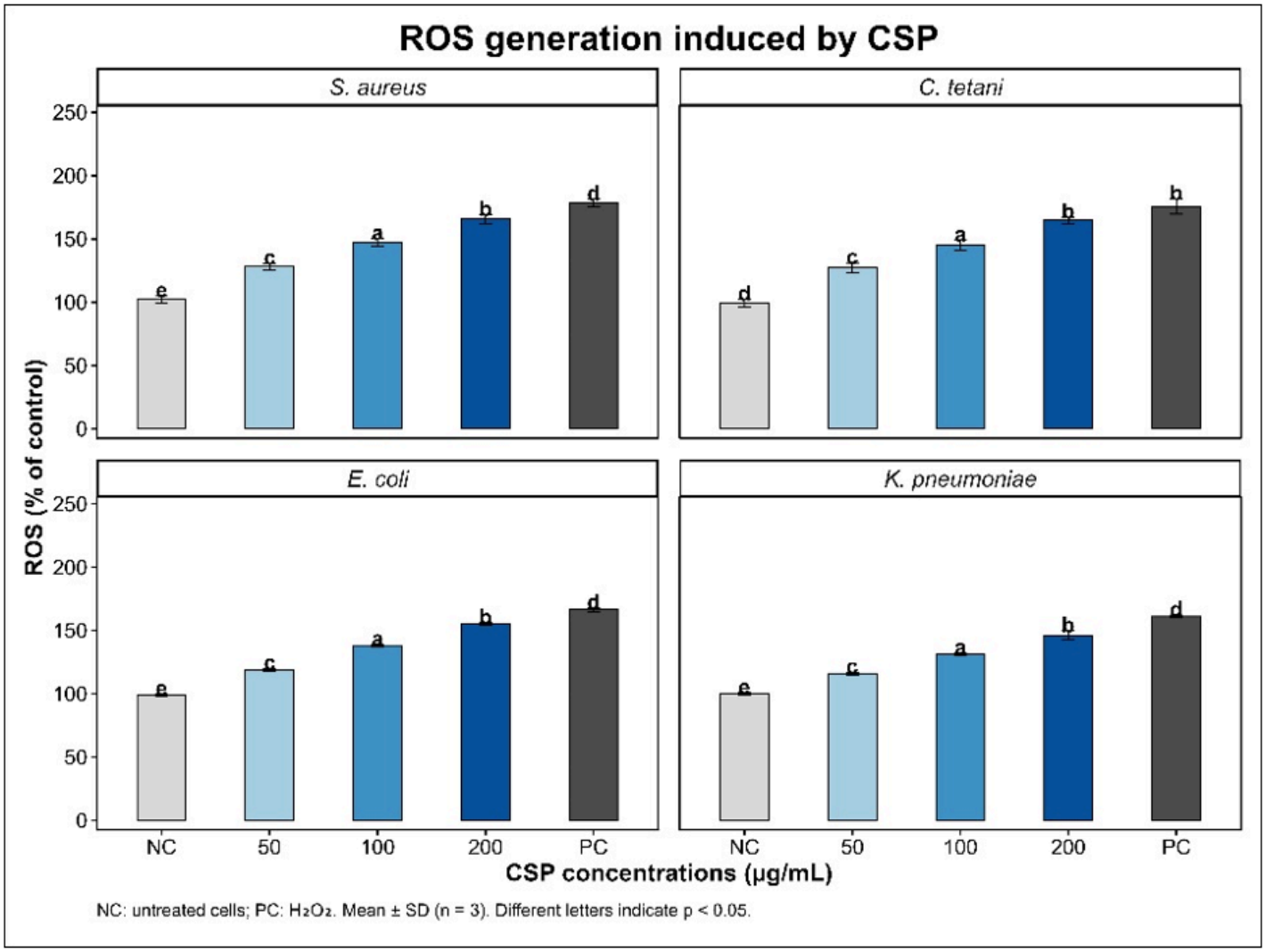

Figure 11

Figure 10a. Intracellular ROS generation in bacterial strains treated with CSP at different concentrations (50-200 µg/mL), measured using the DCFH-DA assay and expressed relative to the untreated control.

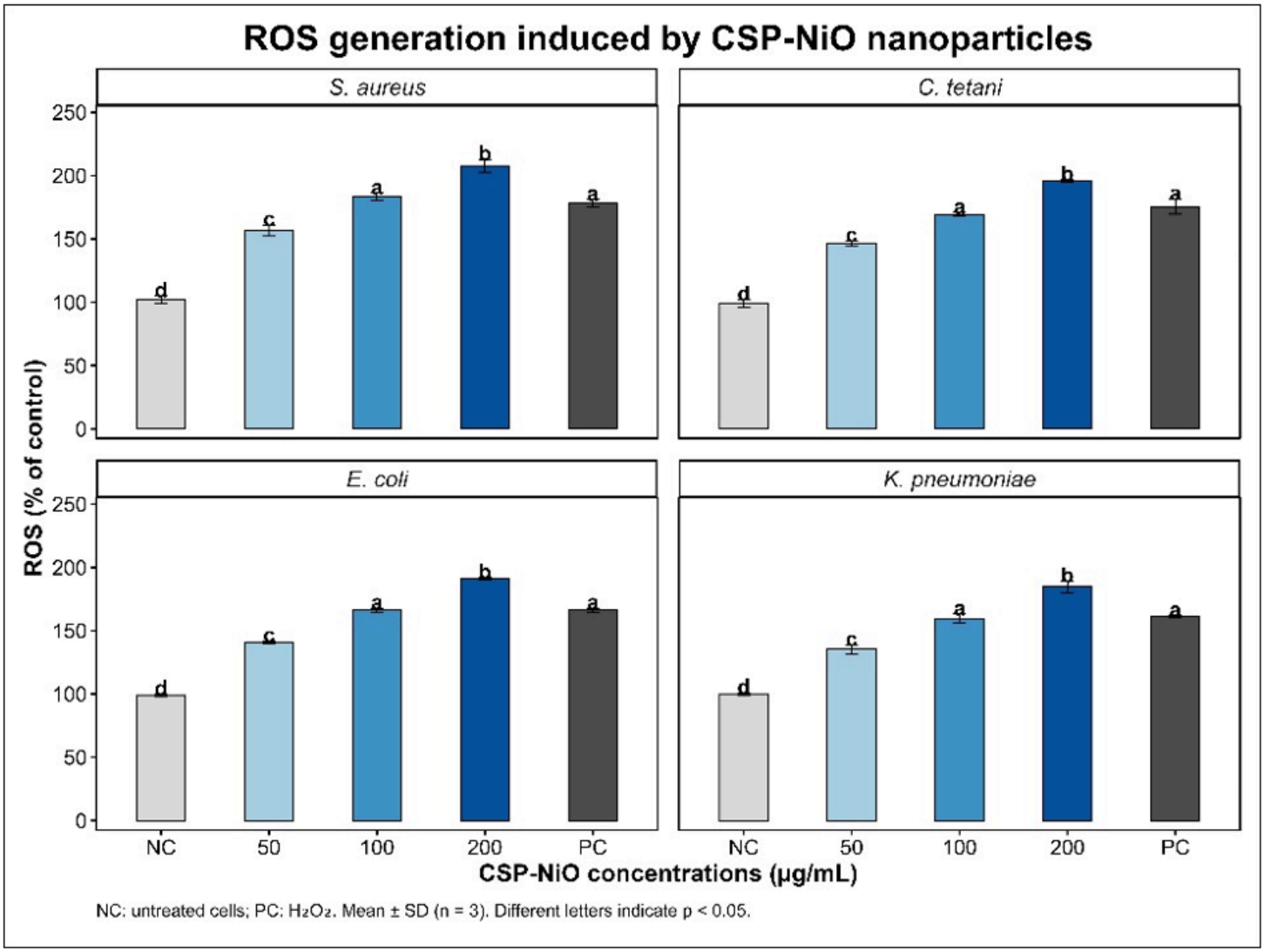

Figure 12

Figure 10b. Intracellular ROS generation in bacterial strains treated with CSP-NiO nanoparticles at different concentrations (50-200 µg/mL), measured using the DCFH-DA assay and expressed relative to the untreated control.

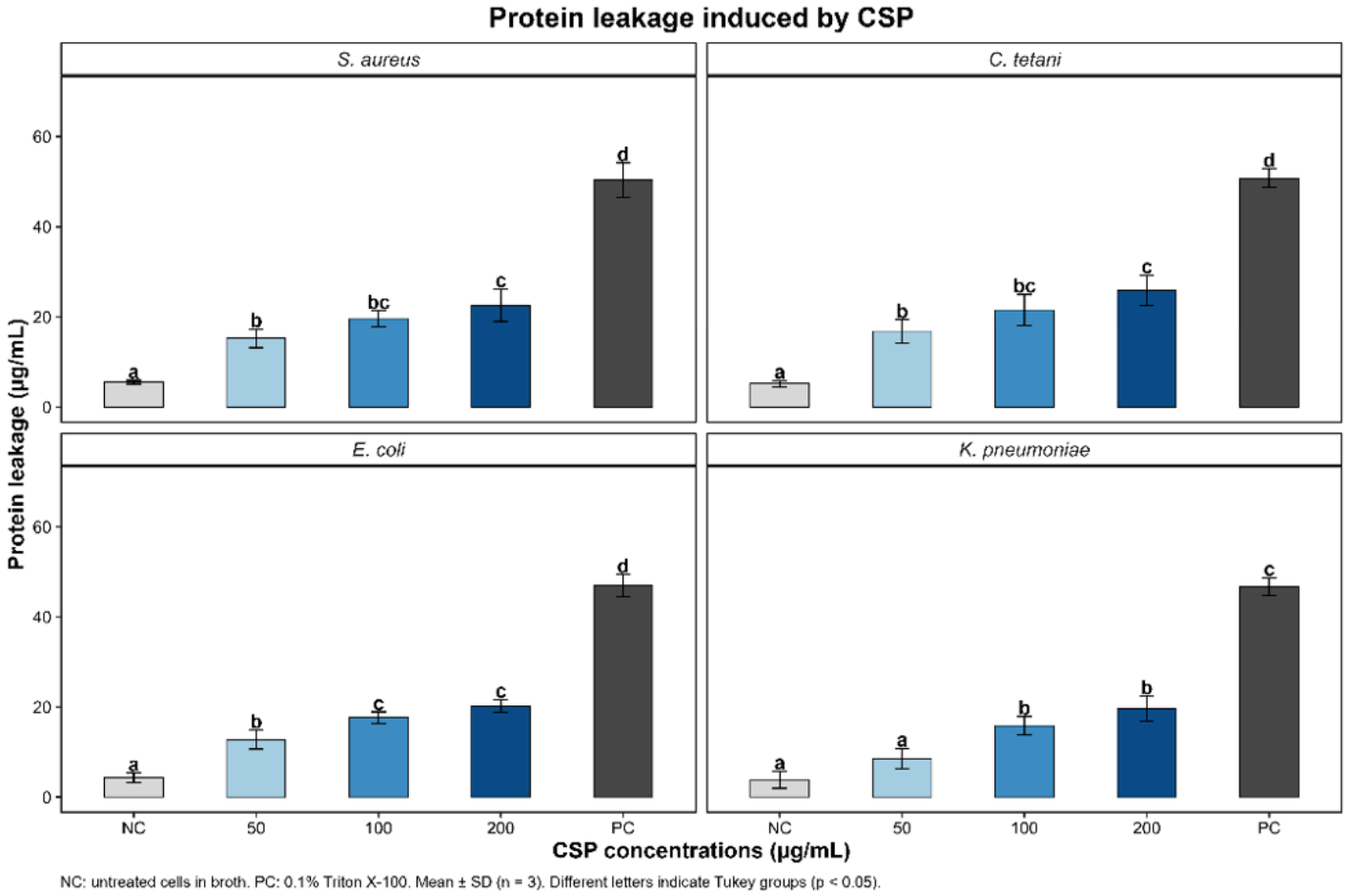

Figure 13

Figure 11a. Protein leakage in pathogenic bacterial strains induced by CSP at different concentrations (50-200 µg/mL) after 6-hour exposure.

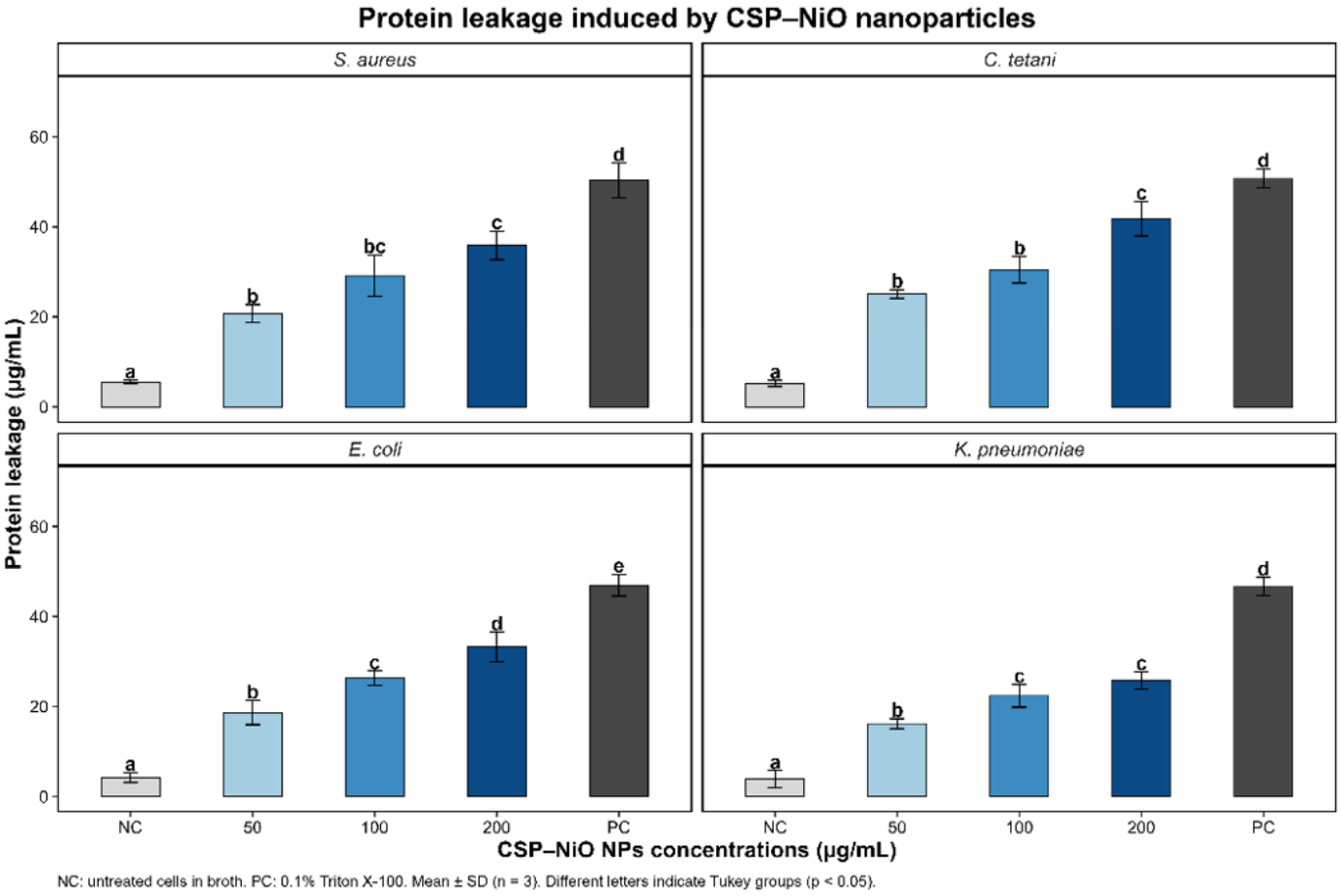

Figure 14

Figure 11b. Protein leakage in pathogenic bacterial strains induced by CSP-NiO nanoparticles at different concentrations (50-200 µg/mL) after 6-hour exposure.

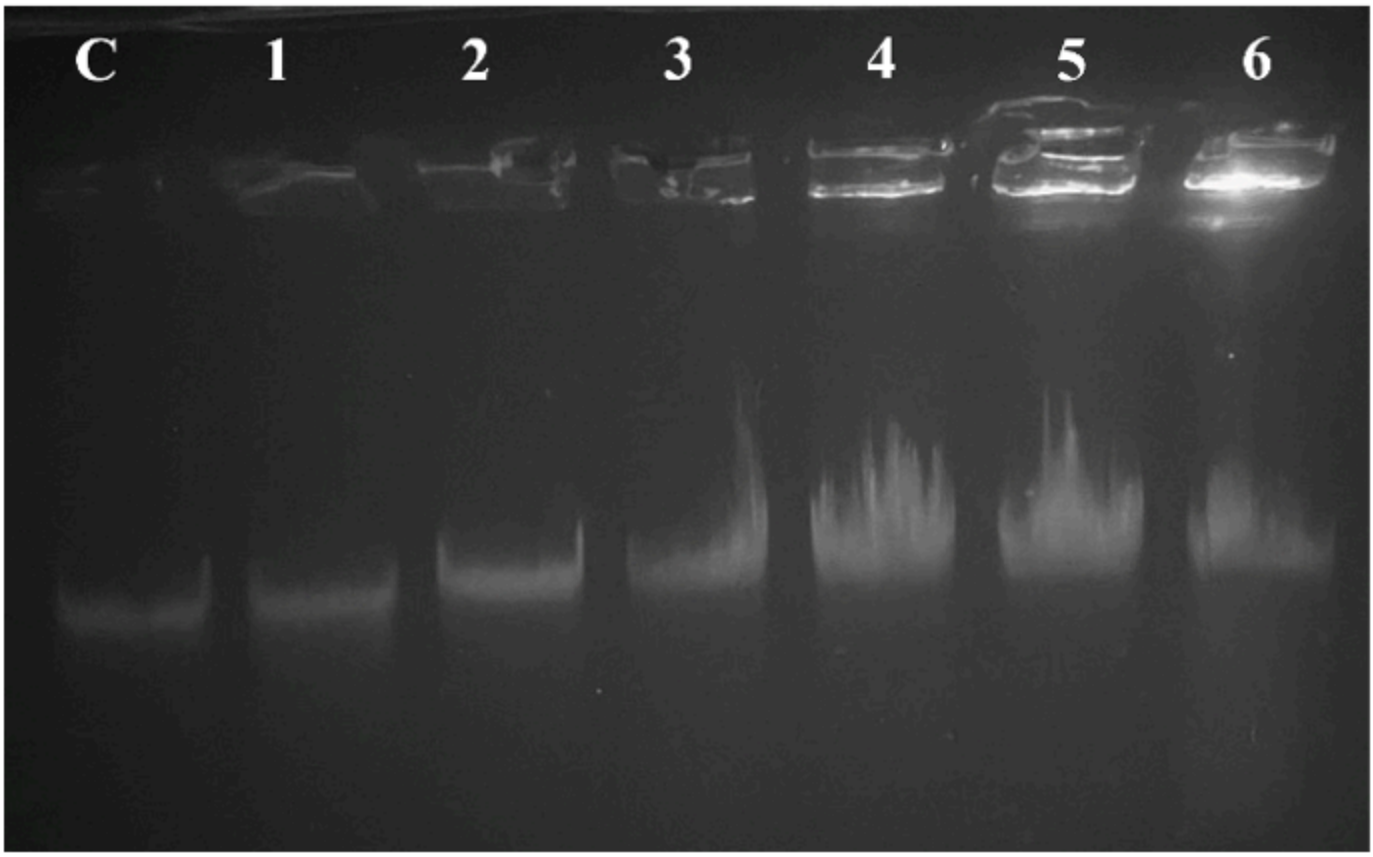

Figure 15

Figure 12. Bacterial DNA fragmentation by CSP and CSP-NiO nanoparticles. Lane C: negative control (untreated cells); Lanes 1-3: CSP-treated cells at 50, 100, and 200 µg/mL, respectively; Lanes 4-6: CSP-NiO-treated cells at 500, 100, and 200 µg/mL, showing enhanced DNA disruption compared to the control.